Phosphorylation motif dictates GPCR C-terminal domain conformation and arrestin interaction

Myriam Guillien, Assia Mouhand, Amin Sagar, Aurélie Fournet, Frédéric Allemand, Glaécia A.N. Pereira, Aurélien Thureau, Pau Bernadó, Jean-Louis Banères, Nathalie Sibille

Phosphorylation motif dictates GPCR C-terminal domain conformation and arrestin interaction

Myriam Guillien,[1,†] Assia Mouhand,[1,†] Amin Sagar,[1] Aurélie Fournet,[1] Frédéric Allemand,[1] Glaécia A. N. Pereira,[2] Aurélien Thureau,[3] Pau Bernadó,[1] Jean-Louis Banères,[2] Nathalie Sibille,[1,4,*]

[1]Centre de Biologie Structurale (CBS), CNRS, Univ. Montpellier, Inserm, Montpellier, France
[2]Institut des Biomolécules Max Mousseron (IBMM), UMR-5247, Univ. Montpellier, CNRS, ENSCM, Montpellier, France
[3]HélioBio Section, Synchrotron SOLEIL, L'Orme des Merisiers, Saint-Aubin BP 48, 91190 Gif-sur-Yvette, France
[4]Lead contact
† These authors contributed equally to this work
*Correspondence: nathalie.sibille@cbs.cnrs.fr

In brief

Arrestin recruitment to the phosphorylated C-terminal domains of GPCRs is a central event in signaling. However, the molecular processes responsible for such a recruitment remain elusive because of the high flexibility of these receptor domains. Here we combined state-of-the-art biophysical methods with model GPCRs to illuminate how phosphomimetics impact on the structural dynamics of the receptor C-terminal regions and how this in turn affects the interaction with arrestins. The data emerging from this study clearly point a model where the conformational transitions of the GPCR C-terminal domains associated to their selective charge distribution would play a central role in receptor:arrestin coupling, and therefore could drive arrestin-mediated signaling.

Highlights

- C-terminal domains of GPCRs are intrinsically disordered regions with transient structurations
- Charges distribution in the C-terminal domains of GPCRs induce conformational transitions
- Structural transitions occur in the region that interacts with arrestin-2

Graphical Abstract

Keywords

GPCR; arrestin; Intrinsically Disordered Proteins or Regions (IDPs/IDRs); NMR; interaction;

SUMMARY

Arrestin dependent G protein-coupled receptor (GPCR) signaling pathway is regulated by the phosphorylation state of GPCR's C-terminal domain, but the molecular bases of arrestin:receptor interaction are to be further illuminated. Here we investigated the impact of phosphorylation on the conformational features of the C-terminal region from three rhodopsin-like GPCRs, the vasopressin V2 Receptor (V2R), the Growth Hormone Secretagogue or ghrelin Receptor type 1a (GHSR) and the β2-Adernergic Receptor (β2AR). Using phosphomimetic variants, we identified pre-formed secondary structure elements, or short linear motif (SLiMs), that undergo specific conformational transitions upon phosphorylation. Of importance, such conformational transitions appear to favor arrestin-2 binding. Hence, our results suggest a model in which the phosphorylation-dependent structuration of the GPCR C-terminal regions would modulate arrestin binding, and therefore signaling outcomes in arrestin dependent pathways.

INTRODUCTION

Arrestins are key regulators of G Protein-Coupled Receptor (GPCR) signaling. They are involved in receptor desensitization and internalization, and act as scaffolds [1]. How these distinct functions are specifically triggered upon GPCR activation remains an open question. It has been proposed that the outcome of arrestin signaling depends on the phosphorylation state of active receptors, leading to the so-called phospho-barcode model [2–4]. This model states that, upon activation by their ligand, GPCRs are phosphorylated at different sites on their C-terminal domain (GPCR-Cter), and intracellular loops [5,6]. This impacts the way GPCRs interact with arrestin, in turn affecting arrestin conformation and, ultimately, the intracellular signal triggered by arrestin. More recently, atomic-resolution structures of GPCR:arrestin complexes have revealed different organizations of arrestins [7–10]. However, because of the diversity in the experimental conditions used in these studies, these structures still hardly support the barcode hypothesis, which thus remains essentially supported by functional studies [3,11–13]. Additionally, based on the crystal structure of the rhodopsin:arrestin complex, Zhou and co-workers proposed a set of phosphorylation motifs required for the high-affinity binding to arrestin [8]. These phosphorylation motifs correspond to a long p[S/T]XXp[S/T]XXp[S/T]/E/D motif or a short p[S/T]Xp[S/T]XXp[S/T]/E/D motif, where p[S/T] represents a phospho-serine or -threonine, X is any amino acid except proline in the second XX occurrence. More recently, a PXPP-type phosphorylation motif found in many different GPCRs has been shown to be recognized by a complementary sequence on arrestins [14]. These motifs seem to be conserved across the major GPCR subfamilies despite the very low sequence conservation of their C-terminal domains. [8,15,1615]

There is still a lack of experimental data explaining how GRK phosphorylation affects the C-terminal domain of GPCRs and leads to different interactions with arrestin, as only structures of class B receptors, which interact more strongly with arrestin, or chimeric class A receptors with the C-terminus of V2R (V2Rpp), have been reported in the literature until now [7,10,17–19]. Interestingly, GPCR C-terminal domain presents all the structural, dynamic and functional characteristics of an intrinsically disordered region (IDR) [20–23]. Intrinsically disordered proteins (IDPs) or IDRs are highly flexible with a low content of secondary structure, whose specific role in fundamental signaling and regulation processes started to be revealed two decades ago [24–26]. We have previously used Nuclear Magnetic Resonance (NMR) to describe the transient secondary structure contents of the C-terminal domains from three GPCRs: the vasopressin V2 Receptor (V2R) (from residue 343 to 371), the Growth Hormone Secretagogue or ghrelin Receptor type 1a (GHSR) (from residue 339 to 366) and the β2-Adernergic Receptor (β2AR) (from residue 342 to 413) [27]. We thus provided structural information of two class A receptors (GHSR and β2AR), which interact transiently with arrestin and one class B receptor (V2R) which is a common model for receptors interacting strongly with arrestin.

We analyzed here how phosphorylation could affect the structural features of the C-terminal regions of these three receptors. To this end, we produced the corresponding isolated C-terminal domains as non-phosphorylated (wt) and phosphomimetic (pm) recombinant peptides. [19,282930–32]We then used an integrated biophysical strategy combining Size Exclusion Chromatography-Multi Angle Light Scattering (SEC-MALS), Circular Dichroism (CD), solution-state NMR and Small Angle X-ray Scattering (SAXS) to explore the conformational features of these peptides. We provided evidence suggesting the occurrence

of transient β-strand conformations in the phosphomimetic peptide (pm) that were not observed in their unmodified counterparts. We then leveraged florescence and NMR spectroscopy and molecular dynamics (MD) to assess their impact in the interaction with recombinant arrestin-2. The data obtained indicate that these transient structures are indeed directly involved in arrestin binding. Moreover, these highlighted binding regions contained motifs described as putative phosphorylation motif, in line with the above-mentioned models of interaction. Altogether, our results suggest that GRK phosphorylation could induce the formation of a transient β-strand in the C-terminal domains of GPCRs that may serve as a recognition element for arrestin.

RESULTS

Structural characterization of the phosphomimetic forms of the three GPCR C-terminal domains

In order to study the effect of GRK phosphorylation on the conformation of the C-terminal domains of GPCRs (GPCR-Cters), we used three different receptors, i.e., the vasopressin V2 Receptor (V2R), the ghrelin receptor (GHSR) and the β2-Adernergic Receptor (β2AR), as models. These receptors belong to the A (β2AR, GHSR) and B (V2R) classes of GPCRs with regard to the interaction with arrestins, where class A interact transiently and class B more tightly [33]. These GPCR-Cter were produced in *E. coli* as phosphomimetic variants (pm-GPCR-Cter). The phosphomimetic (pm) variants were designed by replacing with glutamic acids all the serines and threonines reported in the literature to be phosphorylated [4,28,34,35] (Fig. 1a).

A combined SEC-MALS, CD and NMR analysis showed that these pm variants are monomeric and disordered domains with transient secondary structures (Fig. 1), as is the case of their non-phosphorylated (wt-GPCR-Cter) forms [27]. Indeed, SEC-MALS profiles of pm variants (Fig. 1b) revealed a single peak for each GPCR-Cter eluting at volume close to that of standard proteins with a molecular mass larger than 13 kDa. This behavior on a SEC column is typical of disordered protein [36]. In contrast, the masses derived from MALS analysis (solid black line) are 3.7 kDa (± 2.4 %) for V2R-Cter, 3.8 kDa (± 1.8 %) for GHSR-Cter and 8.3 kDa (± 0.8 %) for β2AR-Cter (Fig. 1b), which is in agreement with their monomeric molecular weight of 3.6, 3.7 and 8.5 kDa, respectively. This was confirmed by mass spectrometry (MS).

The far-UV CD spectra of the pm variants present a minimum around 200 nm and a shoulder at 220 nm characteristic of disorder proteins with transient secondary structure contents [37] (Fig. 1c). Moreover, ^{15}N-HSQC spectra of pm-V2R-Cter, pm-GHSR-Cter and pm-β2AR-Cter showed a low proton spectral dispersion, typical of IDPs [38] (Fig. 1d). These observations were further confirmed by SAXS where the Kratky plots displayed the typical profile of an IDP with no clear maximum and a monotonous increase along the momentum transfer range (Fig. S1) [38–40].

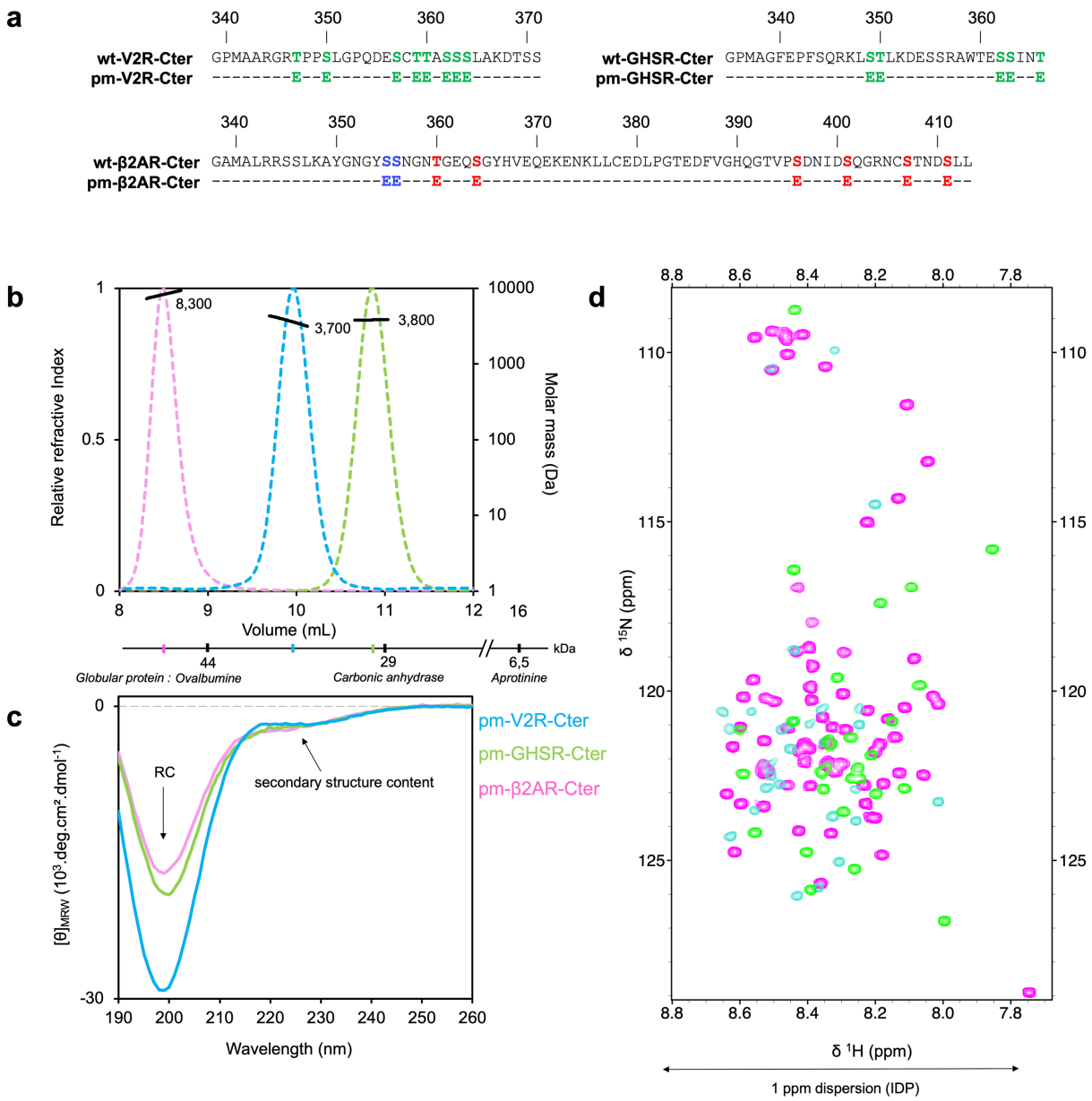

Fig 1. V2R-Cter (blue), GHSR-Cter (green) and β2AR-Cter (pink) phosphomimetic (pm) variants are monomeric and disordered with transient secondary structures. The color code will be maintained for all panels and Figures. **a** Sequence of the GPCR-Cters in their non-phosphorylated (wt) and phosphomimetic (pm) form. Phosphorylated sites by GRK2 (red), GRK6 (blue) or any GRK (green) reported in the literature for β2AR [4], GHSR [34], and V2R [28] are indicated in the wt sequence. These sites were mutated to glutamic acid (E) in the pm variants. **b** SEC-MALS profiles (colored dashed lines) of the pm variants. Elution volume of GPCR-Cters are smaller than that of globular proteins of the same weight, which is characteristic of elongated/disordered proteins. As a comparison, elution volumes of globular Ovalbumine, Carbonic anhydrase and Aprotinine proteins are indicated under the volume axis. **c** Far-UV Circular Dichroism (CD) spectra (colored lines) of pm variants. **d** Overlay of the ^{15}N-HSQC spectra of the pm variants.

To localize and identify transient secondary structures [41], we then performed an NMR study. The backbone assignments were first performed for the three phosphomimetic variants (pm) (Fig. S2a-b) (BMRB accession codes: **51319**, **51328** and **51330** for pm-β2AR-Cter, pm-GHSR-Cter and pm-V2R-Cter respectively). We then used NMR to assess the structural features of the C-terminal domains in their phosphomimetic (pm) form and compared them to their non-phosphorylated (wt) form [27]. C-terminal domains were not affected by the protein concentration, as assessed by NMR (Table S1, Fig. S2c).

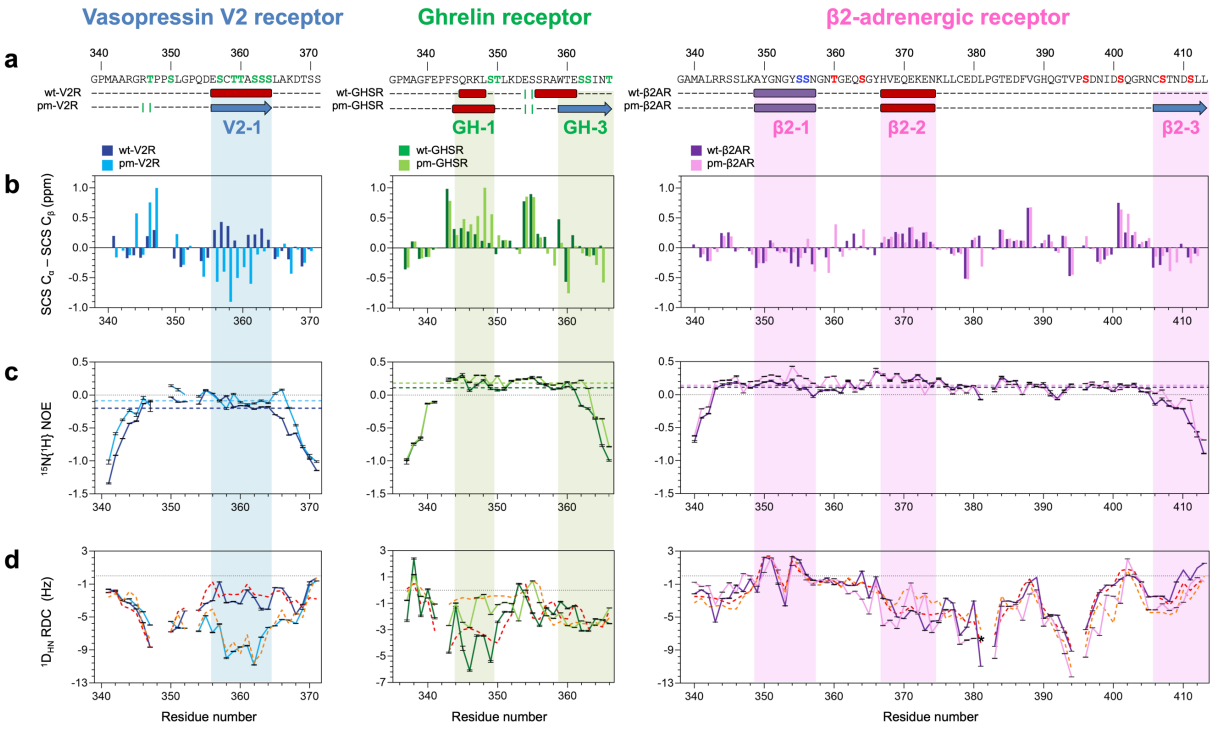

Fig. 2 Comparison of the structural features of the GPCR C-terminal domains (V2R-Cter: blue, left; GHSR-Cter: green, middle; and β2AR-Cter: purple, right) in their non-phosphorylated (wt, dark color, data from [27]) and phosphomimetic form (pm, light color). a Schematic secondary structure consensus of all NMR data along the primary sequences. Known phosphorylation sites mutated to glutamic acid (E) in the variants (pm) are indicated in green, red and blue on the sequence (according to Fig. 1). Helix, β-strand, extended conformation (β-strand or polyproline helix 2, PPII) and turns are represented as red cylinder, blue arrow, purple box and green bars, respectively. **b** Computed secondary chemical shift SCS Cα – SCS Cβ. **c** $^{15}N\{^{1}H\}$ heteronuclear NOEs profiles from the ratio of intensities measured in saturated (I) and unsaturated (I_0) spectra. Averages are in dash colored line. **d** Experimental and back-calculated $^{1}D_{NH}$ RDC. Comparison of experimental RDCs measured in bacteriophage Pf1 for GHSR-Cter, alcohol mixtures for V2R-Cter and β2AR-Cter. Back-calculated RDCs from biased ensembles generated with FM (dashed lines) for wt (red) and pm (orange). The peak displaying signal overlap was removed (dark star).

pm-V2R-Cter. The V2R-Cter phosphomimetic variant presented a large stretch with negative ^{13}C Secondary Chemical Shift (SCS) values (Fig. 2b), from residues 356 to 364 (called V2-1), suggesting a transient β-strand conformation in this region. Interestingly, we showed previously that V2-1 contained a transient helical conformation in the non-phosphorylated form (wt-V2R-Cter) [27]. This loss of helical content between the wt and the pm variant was also substantiated by the decrease of in the percentage of $^{3}J_{HNHA}$ scalar coupling bellow 6 Hz (Fig. S3a), with the majority of scalar couplings remaining in the disordered range between 6 and 8 Hz. Another difference in the SCS profile appeared for residues 346-347 where the pm variant presented highly positive values compared to the wt peptide, certainly related to the presence of a turn. In terms of dynamics, V2-1 relaxation rates R_1 and R_2 displayed lower values for the variant compared to the wild type (Fig. S4c-d). This could be explained by the fact that the β-strand conformation in pm-V2R-Cter is structurally less constrained than the α-helix in wt-V2R-Cter, even though this change in dynamics was not observed in heteronuclear $^{15}N\{^{1}H\}$-NOE (Figs. 2c and S4b). Residual Dipolar Couplings (RDC) also indicated the presence of a transient β-strand conformation in the V2-1 region of the variant. The RDCs profile exhibited more negative values in the V2-1 region of the phosphomimetic (pm) variant compared to the non-phosphorylated (wt) form (Figs. 2d and S5), confirming the transient β-strand conformation in this V2-1 region.

pm-GHSR-Cter. The SCS profile of the GHSR-Cter phosphomimetic (pm) variant revealed the presence of a transient α-helix (from residues 345 to 348 - called GH-1) and a transient β-strand conformation (from 359 to 366 - called GH-3) with positive and negative SCS values, respectively (Fig. 2b). Previously, we identified two transient helices for the non-phosphorylated (wt) form, i.e. GH-1 (from residues 345 to 348) and GH-2 (from residues 356 to 361) (Fig. 2a) [27]. SCS values of the pm variant in the GH-1 region were higher than in the wt peptide, suggesting a stronger helical structuration. Interestingly, GH-2 transient helix found in the wt peptide was shifted downstream and converted to a transient β-strand conformation (GH-3) (Fig. 2b). The transition from a helical to a β-strand transient conformation was confirmed by the decreased of $^{3}J_{HNHA}$ scalar couplings with less than 6 Hz (from 46% to 29%) and a small increase of couplings larger than 8 Hz (from 3% to 4%) between the wt and the pm forms (Fig. S3a). Also, scalar couplings in GH-3 were higher for the pm variant than for the wt peptide, which is in line with a tendency to form a β-strand conformation (Fig. S3b). Dynamic parameters showed an increase of rigidity in GH-1 and GH-3 regions for the pm variant, with higher averaged heteronuclear NOE (0.18 ± 0.01) and transversal relaxation R_2 rate (3.33 ± 0.04 Hz) compared to the wt (0.11 ± 0.01 and 3.17 ± 0.06 Hz, respectively) (Figs. 2c and S4). Conformational changes between the wt and pm peptides were also highlighted by RDC measurements. In agreement with SCS data, the comparison of RDC profiles showed an increase in RDCs in GH-1 and a slight decrease in GH-3 (Fig. 2d), suggesting a stronger helical structuration in GH-1, and a switch and shift from a helical (wt) in GH-2 to a β-strand transient conformation (pm) in GH-3.

pm- β2AR-Cter. The SCS profile of the β2AR-Cter pm variant highlighted three regions with negative and positive values indicating transient secondary structures: an extended conformation from residues 349 to 357 (called β2-1), a transient helix from residues 368 to 376 (called β2-2) and a transient β-strand conformation from residues 407 to 413 (called β2-3) (Figs. 2 and S3-S5). The NMR characterization of the wt peptide gave similar results for the two first regions [27] while no secondary structure was observed in the third one (Fig. 2B). The appearance of a transient β-strand in β2-3 was manifested by the increase in the $^{3}J_{HNHA}$ values between 7 and 8 Hz (from 13 to 28 %) (Fig. S3). Moreover, in this region, heteronuclear NOE and transversal relaxation R_2 data showed a slight increase in their values for the pm variant compared to the wt form, while the longitudinal relaxation R_1 remained unchanged (Figs. 2C and S4). These results suggested a local structuration and reduced conformational mobility in agreement with the presence of a transient secondary structure in β2-3. The emergence of β2-3 was also observed in the RDC analysis, as RDCs adopted more negative values in β2-3 for the pm variant compared to the wild type, again suggesting the presence of a transient β-strand conformation (Figs. 2d and S5). Altogether, comparison of all β2AR-Cter's NMR data in their non-phosphorylated (wt) and phosphomimetic (pm) forms confirmed a conformational transition of the β2-3 region from a random coil (non-phosphorylated form) to a transient β-strand (phosphomimetic form) (Fig. 2a). Finally, no drastic changes were observed in the long-range interaction previously identified in wt-β2AR-Cter (Fig. S6).

Conformational ensemble of the GPCR-Cters phosphomimetic forms. To go further in the description of the pm-GPCR-Cter conformations, we generated random-coil ensembles of 50,000 conformers for each pm variant using Flexible Meccano (FM) [42,43]. The quality of these ensembles was evaluated by comparing back-calculated to experimental RDCs. Back-calculated RDCs from random-

coil ensemble showed discrepancies with the experimental ones for all pm variants, especially in the transient beta-stranded regions V2-1, GH-3 and β2-3 (Fig. S5b). Thus, we included conformational preferences defined by NMR data in biased ensembles of 50,000 conformers (Figs. 2d and S5b). The best agreement for the pm-V2R-Cter ensemble (χ^2 = 1.23) was found when imposing 10%, 50% and 25% of β-strands for residues 352-357, 359-362 (V2-1) and 364-368, respectively, (Fig. S5b), while wt-V2R-Cter ensemble revealed a 5% helix content in V2-1. Thus, ensemble description of V2R-Cter clearly confirmed the conformational change between pm- and wt-V2R-Cter and a strong propensity of the pm variant to adopt a transient β-strand conformation in V2-1. In addition, the two poly-proline II helices (PPII) identified in the non-phosphorylated (wt) ensemble were also added in position 344-345 (20%) and 350-351 (30%) of the pm-variant. In the best ensemble of pm-GHSR-Cter (χ^2 = 0.77), the major difference between the pm variant and the wild-type ensembles was the introduction of 60% of β-strand in GH-3 (Fig. S5b) instead of 8% of helix in GH-2, respectively. It confirmed the structural transition from a transient helix (wt) to a transient β-strand (pm) in GHSR-Cter. In addition, a stronger helical structuration was observed in GH-1 in the variant (4% of helix from 349 to 351) (Fig. S5b), compared to the wild-type ensemble, where no conformational bias was required in this region. For the β2AR-Cter variant, the best ensemble (χ^2 = 4.21) was obtained by imposing 5% of β-strand near β2-3 region (Fig. S5b), while no conformational constraints were added in this region for the wild type. This result showed that the conformational change to a transient β-strand also occurred in β2AR-Cter variant but to a lower extent than in the two other Cters. Another difference appeared in β2-2 region where 5% helix was added instead of a PPII in the wild type. The ensemble of the pm variant was also constrained by a 10% β-turn I in residues 401-402 (Fig. S5b). For both the pm- and the wt-β2AR-Cter, a long-range contact (15 Å) was incorporated to the model. Indeed, decreases in the PRE ratio were identified between regions surrounding β2-1 (residues 338-357) and β2-2 (residues 367-386) (Fig. S5c) for both the pm- and the wt-β2AR-Cter. Altogether, wild-type ensembles show a conformational transition that occurs when introducing phosphomimetic residues and involves larger populations of β-strand conformations.

Interaction of the C-terminal domain of GPCRs with Arrestin

To assess the functional impact of the conformational changes described above, we then analyzed the interaction of the three GPCR-Cter peptides with their major biological partner, arrestin.

Arrestin binding sites contain putative phosphorylation motifs. NMR is a suitable tool to study the location and strength of transient interactions by monitoring the changes in chemical shift and/or intensity of a labeled protein in the presence of increasing amounts of the unlabeled partner [44,45]. To this end, we recorded a set of ^{15}N-HSQC spectra of ^{15}N labeled GPCR-Cters incubated with different ratios of unlabeled arrestin-2 to perform a Chemical Shift Perturbation (CSP) assay. 1H/15N chemical shift perturbations (CSP) indicates a change in the chemical environment of the peptides due to the presence of the partner arrestin, and possibly transient hydrogen bond formation, which were also observed in our molecular dynamics simulations (see below). To be noted, the difference in the tumbling rate between the free peptide and its transient complex with arrestin-2 likely affects the intensity of the NMR peaks of the interacting regions. Indeed, upon interaction the overall tumbling of the interacting region of the peptide increases, causing a decrease in the intensity of the residues involved. In the absence of

chemical exchange processes, the attenuation of peaks in the interacting region will thus depend on the affinity and kinetics of the complex formation and it is in line with the degree of chemical shift perturbation (CSP) (Fig. S7). For the three phosphomimetic variants, changes in chemical shifts were observed when comparing the spectra of the protein in the absence and presence of arrestin-2 (respectively 1:0 and 1:10) (Fig. S6). For the pm-V2R-Cter, chemical shift changes and an intensity decrease proportional to the amount of added arrestin-2 were observed for residues 356 to 366 (Figs. 3 and S7a). Similar results were obtained for pm-GHSR-Cter for residues 358 to 366 (Figs. 3 and S7b). Regarding pm-β2AR-Cter, small chemical shift changes were observed for residues 408-413 at a 1:10 ratio (Figs. 3 and S7c). Importantly, no interaction was observed between the three non-phosphorylated C-terminal domains (wt-GPCR-Cter) and arrestin-2, highlighting the importance of phosphorylation for arrestin recognition of GPCRs (Figs. 3 and S6-S7).

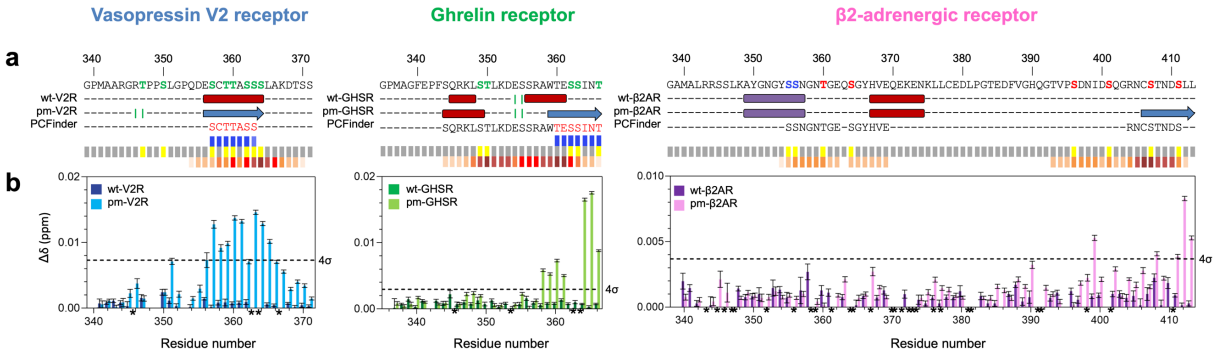

Fig. 3 Interaction between arrestin-2 and the C-terminal domains of V2R-Cter (blue, left), GHSR-Cter (green, middle) and β2AR-Cter (purple, right) in their non-phosphorylated (wt, dark colors) and phosphomimetic (pm, light colors) forms. For each receptor: **a** sequence of the C-terminal domain is indicated according to Fig. 1 and just below successively, secondary structure contents of non-phosphorylated (wt) and phosphomimetic (pm) variants, and predicted phosphorylation motifs (PCFinder = PhosCoFinder [8]); (in the middle) putative phosphorylation motifs (p[S/T](X)Xp[S/T]XXp[S/T]/E/D motifs) displayed on three different tracks: blue track contain the complete motifs (motif containing three negatively charged residues), grey track contain the sequence with the known phosphorylation sites from Uniprot and PhosphoSitePlus database [46] in yellow, reddish track contain partial motifs (motif containing two negatively charges residues instead of three). For partial motifs, darker colors indicate residues involved in multiple motifs. **b** $^{1}H/^{15}N$ Chemical Shift Pertubation (CSP) observed at ratio 1:10 (10 µM GPCR-Cter:100 µM arrestin) aligned with the putative phosphorylation motifs. CSP were recorded on a ^{15}N-labeled GPCR-Cter sample at 10 µM in the absence or in the presence of unlabeled arrestin-2 at 100 µM of at 800 MHz and 20 °C in a 50 mM Bis-Tris pH 6.7, 50 mM NaCl buffer. Cut-offs are in black dashed lines and peaks displaying signal overlap were removed (dark star).

Noteworthy, the identified binding regions overlapped with the regions undergoing a conformational transition between the non-phosphorylated (wt) and the phosphomimetic (pm) variants (Fig. 3). Moreover, these regions were also predicted to contain phosphorylation motifs when using the server PhoCoFinder [8]. These phosphorylation motifs were proposed as motifs required for high-affinity arrestin binding. For pm-V2R-Cter and pm-GHSR-Cter, the binding region encompassed a so-called complete phosphorylation motif (three negatively charged residues), while pm-β2AR-Cter contained only a partial phosphorylation motif (two negatively charges residues instead of three) (Fig. 3). This was in line with the short binding region with a weaker chemical shift perturbation (0.009 ppm ± 0.001), suggesting a lower affinity for arrestin-2. On the opposite, the phosphomimetic variant of V2R-Cter experienced the largest chemical shift perturbation with a Δδ of 0.015 ppm (± 0.001) and the largest binding region with a dozen of residues impacted, which should be related to a stronger interaction with arrestin-2. These

observations likely provide the structural bases of the previously reported higher affinity for arrestin of V2R with respect to GHSR1a and β2AR [47].

GRK phosphorylation acts as a switch of GPCR's C-terminal domains conformation. We thus showed that the regions that exhibited a conformational transition from helical or random coil to β-strand were involved in the interaction with arrestin. The interaction with arrestin could be facilitated by a pre-configuration of the C-terminal domain of GPCRs upon GRK phosphorylation or, alternatively, the final configuration could be induced by the folding of the C-terminal domain of GPCRs upon binding of arrestin. We checked whether there was a change in the conformation upon binding of the phosphomimetic variant of V2R-Cter, which exhibits the highest affinity interaction among the three GPCR-Cter studied here. We observed very similar secondary chemical shift (SCS) profiles in the presence and in the absence of arrestin-2 (Fig. 4). This result suggests a conformational selection mechanism rather than a folding upon binding, however an induced fit mechanism in a second instance, which would stabilize the transient pre-structured β-strand, cannot be excluded. This hypothesis was first supported by the observation that the non-phosphorylated forms, which do not encompass neither any charges nor β-strand conformation, did not interact with arrestin. Moreover, in the X-ray structures of GPCR:arrestin complexes available, the bound state of the C-terminal regions of the receptors displayed a β-strand conformation. In this context, it is tempting to suggest that a well-disposed charge configuration governed by the presence of a pre-existing extended structure of the C-terminal domain of GPCRs is necessary for arrestin recognition.

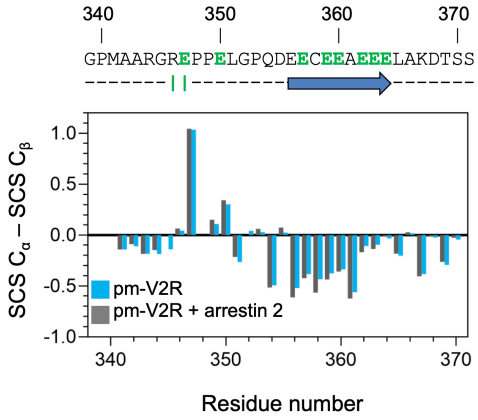

Fig. 4 Conformational selection of phosphomimetic V2R-Cter by arrestin-2. $^{13}C\alpha/^{13}C\beta$ secondary chemical shift (SCS) computed with POTENCI [48,49] of pm-V2R-Cter in absence (blue) or in presence of arrestin (grey). 3D spectra were recorded on $^{13}C/^{15}N$ pm-V2R-Cter (50 µM) in absence or in presence of arrestin-2 (250 µM) at a ratio of 1:5 at 800 MHz and 20 °C in a 50 mM Bis-Tris pH 6.7, 50 mM NaCl buffer.

Arrestin reorganization in the GPCR-Cter:arrestin complexes. We then analyzed if, conversely, interaction with the pm peptides affected the conformational features of arrestin. To this end, we first developed an arrestin-activation sensor based on the FRET signal between a fluorescence donor (AlexaFluor350) and an acceptor (AlexaFluor488) attached to each lobe of purified arrestin-2 (Fig. 5a). The selected positions, *i.e.* V167 and L191, are closely related to those recently shown to report on arrestin activation, based on single molecule fluorescence experiments [50]. Namely, the FRET-signal between fluorescent probes attached to the N- and C-lobes report on the inter-lobe movement

associated to arrestin activation. A significant change in the FRET ratio was observed (Fig. 5b) in the presence of the phosphomimetic peptides, suggesting that the latter interact with purified arrestin and trigger a change in the relative orientation of the arrestin N- and C-lobes. In contrast, no significant change in the FRET ratio was observed for the non-phosphorylated peptides, suggesting that these peptides do not interact with arrestin. However, an interaction that would not be accompanied by a change in the conformation of arrestin cannot be excluded at this stage. To be noted, for the GHSR- and β2AR-Cters, a statistically significant FRET ratio change was observed only at high peptide-to-arrestin molar ratios, suggesting a significantly lower affinity of these peptides compared to the V2R-Cter. However, in all cases, the high excess required to get significant FRET ratio differences suggests a weak interaction between arrestin and the phosphomimetic peptides. This is consistent with the affinity values estimated from microscale thermophoresis (MST) and fluorescence anisotropy experiments that lie in the 200 µM range (Fig. S8), which is in the same range than the values reported for CCR5-derived peptides by solution-state NMR [51].

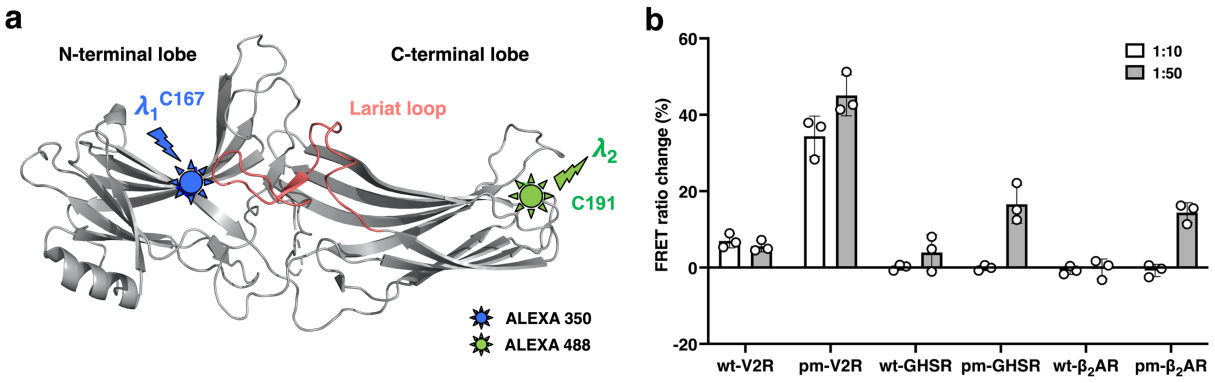

Fig. 5 FRET-monitored interaction between purified arrestin-2 and the non-phosphorylated and phosphorylated Cters. a Structure of arrestin2 (PDB ID: 1G4M) with fluorescence donor (AlexaFluor350) and an acceptor (AlexaFluor488) attached to each lobe. **b** Changes in the FRET ratio measured for the dual labeled arrestin in the absence and presence of the wt peptides (wt-V2R-Cter, wt-GHSR-Cter, wt-β2AR-Cter) and their phosphomimetic counterparts (pm-V2R-Cter, pm-GHSR-Cter, pm-β2AR-Cter) at different arrestin-to-peptide stoichiometric ratios (1:10 or 1:50). Data expressed in % are the mean ± SD of three experiments.

Phosphomimetic peptides mimic the interactions made by phosphopeptides

We finally performed molecular dynamics (MD) simulations to understand the interactions between the phosphomimetic peptides and arrestin-2. To this end, we used the NMR data to define the regions of the peptides that bind to arrestin-2 and generated the initial conformations of only the binding region in complex with arrestin-2 using the structure of V2R phosphorylated peptide (V2Rpp) bound to arrestin-2 (PDB ID: 4JQI) [52]. These conformations were then refined using the FlexPepDock server. This led to the occurrence of a β-sheet in the regions of both pm-V2R-Cter and pm-GHSR-Cter involved in the interaction while pm-β2AR-Cter adopted a less clear β-sheet (Fig. 6). This agrees with the secondary structure determined from the NMR data (Fig. 2 and Fig. S5b). The refinement by FlexPepDock was followed by the addition of the remaining residues of the peptides and performing MD simulations by gradually releasing the restraints from the complex (see Methods). For both pm-V2R-Cter and pm-GHSR-Cter, the β-strand at the primary binding regions was consistently maintained and the interactions

with arrestin-2 via an anti-parallel β-sheet were preserved throughout the simulations (Fig. 6a-b). For pm-β2AR-Cter, the binding region was more flexible and showed occasional detachment and rebinding with more than 90% frames in the bound state. On the other hand, the remaining part of the three peptides showed much more conformational flexibility and made transient interactions with multiple regions of arrestin-2 (Fig. 6a). The probability of contacts between residues of phosphomimetic peptides and arrestin showed that peptides make transient interactions with all the pockets identified on the surface of arrestin (Figs. 7 and S9a). We observed the formation of almost all the hydrogen bonds (H-bonds) present in the crystal structure of V2Rpp [52] including H-bonds with K10-11, R25, K107, K146, K160, R165 and K294 (Fig. 6c).

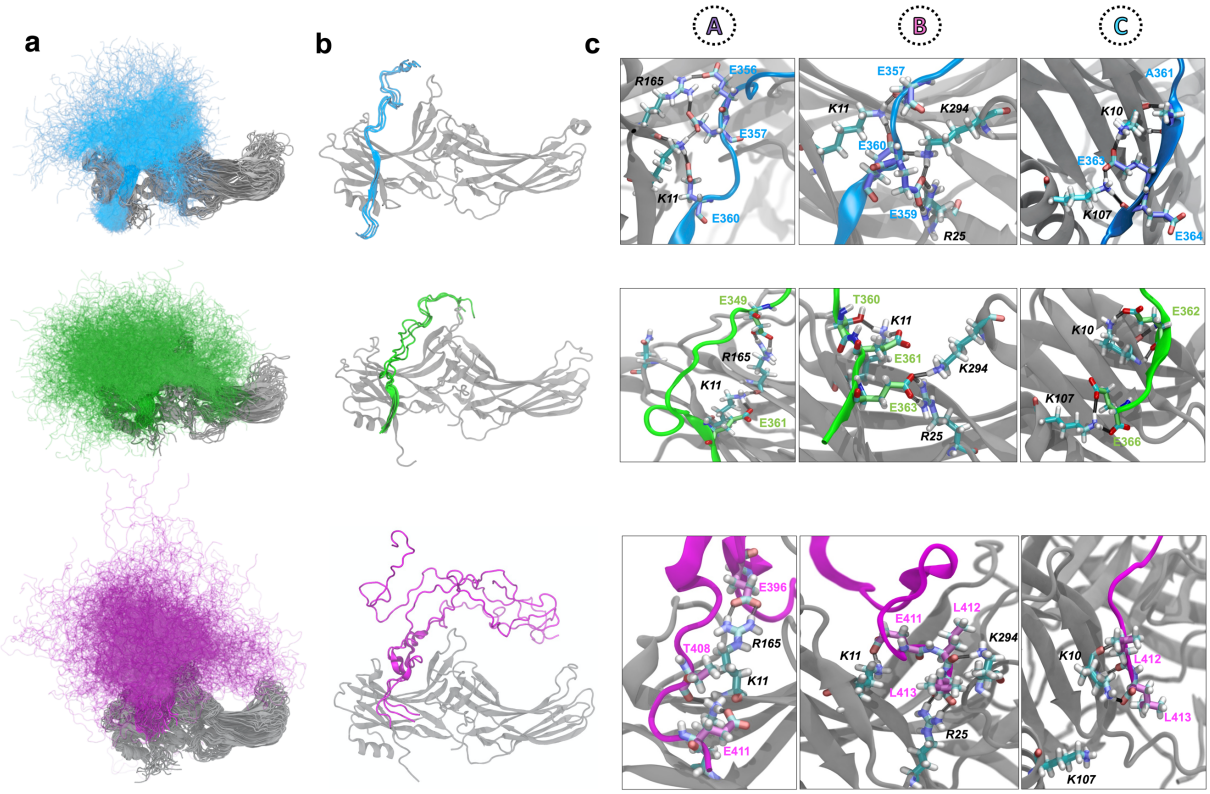

Fig. 6 Modeling of pm-V2R-Cter (blue), pm-GHSR-Cter (green) and pm-β2AR-Cters (pink): arrestin (grey) complexes. a Conformational ensemble obtained from MD simulations for the three phosphomimetic Cter peptides in complex with arrestin. Every 500th conformation from the four independent simulations is shown. **b** Selected conformations of the three phosphomimetic Cter peptides from the calculated ensembles which form the highest number of hydrogen bonds with arrestin. **c** The insets show the different hydrogen bonds formed by the phosphomimetic Cters with arrestin pockets. Arrestin pockets (A, B and C) are described in Fig. 7. Residues from arrestin are labeled in black and residues from the peptides are labeled in their respective colors.

This demonstrates that the phosphomimetic peptides can recapitulate the interactions made by phosphopeptides and are likely to activate arrestin-2 by a similar mechanism (Fig. S10a). Moreover, the truncated C-terminal domain of V2R adopts a similar conformation when it is a continuation of its receptor's amino acid sequence [19], which could support the generality of the proposed mechanism of arrestin binding to rhodopsin like receptors (Fig. S10b). We also observed that the total number of H-bonds between the phosphomimetic peptide and arrestin is the highest for pm-V2R-Cter, then for pm-

GHSR-Cter and finally for pm-β2AR-Cter, which agrees with the experimentally observed affinity trend (Fig. S9b). Interestingly, some of the more subtle features such as the bifurcated salt-bridge observed for K294 with derived V2Rpp [53], which has been shown to be essential for keeping the lariat loop (Fig. 5a) in the active conformation, was also reproduced by pm-V2R-Cter. This bifurcated salt-bridge was formed by E357 and E360 with an additional H-bond with C358 (Fig. S9c).

DISCUSSION

Understanding how GRK phosphorylation of the C-terminal domain of GPCRs (GPCR-Cter) dictates the recruitment of arrestin is pharmacologically and clinically important. Several three-dimensional structures of receptor:arrestin complexes have been obtained so far that provide a first picture of this interaction. However, the picture is still incomplete as these structures do not provide major indications on the dynamics of the interaction. Moreover, they have been obtained for receptors that strongly interact with arrestin, such as class B receptor or phosphorylated rhodopsin with native C-terminus in complex with visual arrestin-1 [8,54], or chimeric class A receptors with the C-terminus of V2R (V2Rpp), which is a class B receptor.

Here, we studied how GRK phosphorylation affects the conformation of GPCR C-terminal domains and their interaction with arrestin-2. To the end, we used C-terminal constructs of the receptor to be able to extract high resolution information of these extremely flexible systems [55]. This strategy of divide and conquer has been previously used in GPCR studies such as the V2pp:arrestin complex [15,52], as well as for other macromolecular complexes [41,56]. We also used phosphomimetics [30] in order to work with a homogeneous system, facilitating the structural characterization [31]. In this approach, phosphorylation of serine and threonine residues is mimicked by mutations to glutamate, which provides the negative charge and has a similar volume. Phosphomimetics have been widely used in protein science to decipher the structural and functional role of phosphorylation [30–32]. However, it cannot be excluded at this stage that, although they mimic the general behavior of phosphorylated S/T, phosphomimetics could have an impact on the affinity of the peptides for arrestin. Importantly, our NMR data provide evidence that the phosphomimetic variants interact with arrestin-2 whereas the non-phosphorylated forms do not, validating the use of phosphomimetic peptides. This result is in line with the fact that phosphorylation is generally necessary for arrestin binding [57]. Moreover, modeling of pm-GPCR-Cter:arrestin complexes and MD simulations show that the binding mode of the phosphomimetic V2R C-terminal domain to arrestin is similar to phosphopeptides [52], or to the whole V2 receptor in complex with arrestin [19]. This further demonstrates the suitability of isolated C-terminal phosphomimetic peptides as models for studying GPCR-arrestin interactions. Besides, as the precise phospho-pattern triggered by individual GRKs is not known for GHSR and V2R, we used here peptides where all the phosphorylation sites reported in the literature were modified. We cannot exclude, at this stage, that these different sites have different impact on the interaction with arrestin. As reported for rhodopsin, different functional classes of phosphorylation sites were observed, with some involved in arrestin binding and activation while others displayed an inhibitory or modulatory effect on the interaction [58].

Our data show that both the non-phosphorylated C-terminal domains and their phosphomimetic counterparts behave in solution as intrinsically disordered regions (IDRs) with transient secondary

structure elements. However, mimicking GRK phosphorylation causes the formation of β-strand conformations in localized segments of the GPCR-Cters, suggesting that the GPCR-Cter functional folding is regulated by GRK phosphorylation, similar to other proteins such as the eukaryotic translation factor 4E-binding protein 2 [59]. Of importance, the transient β-strand conformations in the three C-terminal domains, only present in the phosphomimetic variants, corresponded to the arrestin interacting region (Fig. 3). Interestingly, several atomic resolution structures, obtained by X-ray crystallography and cryo-electron microscopy, showed a β-strand conformation of the fully phosphorylated C-terminus peptide of vasopressin V2 receptor (V2pp), which formed an anti-parallel β-sheet with the N-domain of arrestin-2 [7,9,60,61]. In addition, in the structural arrangement of the parathyroid hormone receptor PTHR1:arrestin-2 complex inferred from in cell cross-linking assays, the bound part of the receptor C-terminal domain appears to be in β-strand [62], supporting the mechanism proposed here.

A similar fold was also observed for the phosphorylated rhodopsin C-terminus (pRho) in interaction with visual arrestin-1 [8,54]. In these complexes, an extensive network of electrostatic interactions exists between the negatively charged residues of the C-termini and three conserved pockets of positive residues in the N-domain of arrestin: A (K19, R22 and R175), B (K19, R33 and K304) and C (K18 and K114) (Fig. 7; residue number corresponding to the human arrestin-1). V2Rpp and pRho β-strands are located between arrestin pockets B and C. However, in a recent X-ray atomic structure showing a synthetic fully phosphorylated peptide of CXCR7 receptor (C7pp) in interaction with arrestin-3 [16], the C-terminal domain of CXCR7 adopted an elongated loop that, in addition to pockets A and B, interacts with a new pocket P (K154 and K170, Fig. 7). Moreover, Yu and collaborators showed that the interaction of phosphate of V2R C-terminus with specific pocket of arrestin affects the interaction surfaces of arrestin with its cytosolic partners [63]. Thus, it is possible that, depending on the conformation of the GPCR C-terminal domain, phosphates do not interact with the same pockets of arrestin, leading to distinct arrestin function. This folding could also be used to select a particular arrestin subtype.

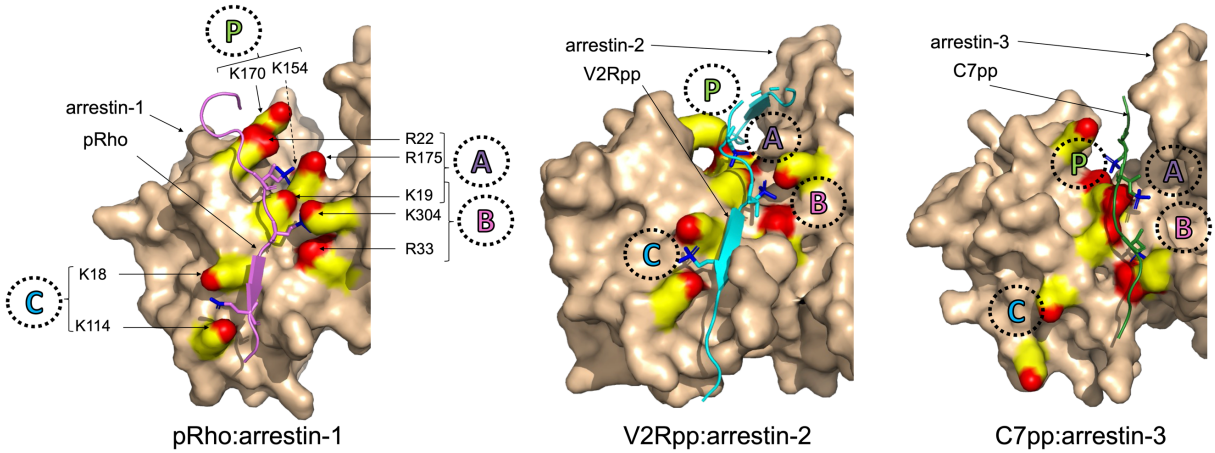

Fig. 7 Atomic structures of GPCR:arrestin complex. For the rhodopsin:arrestin-1 complex [8], the C-terminal domain was phosphorylated during its production in insect cells (pRho); while in the two other complexes, V2R and CXCR7, the C-terminal domain correspond to synthetic fully phosphorylated peptides (respectively V2Rpp and C7pp) [16,52]. V2Rpp and pRho interact with arrestin pocket A (K19, R22 and R175), B (K19, R33 and K304) and C (K18 and K114) while C7pp interacts with pocket P (K154 and K170), in addition of pocket A and B. These pockets are conserved among arrestins and residue numbers correspond to the sequence of human arrestin-1. K154 is localized in a crest behind R175 and is not visible in the figure (dashed arrow).

Binding regions identified in our study contained phosphorylation motifs specific to GPCRs (PhosCoFinder [8] and Fig. 3). These phosphorylation motifs correspond to a long p[S/T]XXp[S/T]XXp[S/T]/E/D motif or short p[S/T]Xp[S/T]XXp[S/T]/E/D motif. It was proposed that the presence of three negatively charged residues (full motifs) increased arrestin interaction [8]. Conversely, the absence of one of the three charges (partial motif) reduces the interaction. The vasopressin V2 and the ghrelin receptors encompass full motifs, while the β2-adrenergic receptor displayed only two clusters of partial motifs (Fig. 3). This was consistent with our NMR observations where V2R-Cter encompassed the largest binding region, whereas β2AR-Cter presented the shortest binding region and the lowest arrestin binding affinity. Low affinities (i.e. in the μM range) were previously reported in the literature for the interaction between phospho-peptides of V2R-Cter and arrestin-2 in the presence of Fab30 antibody [9], and for CCR5-derived peptides measured by solution-state NMR [51]. In addition, it has been already shown in IDPs that multisite phosphorylation modulates their affinity toward partners [64]. For example, successive phosphorylation events of the p53 transcriptional factor increase its recruitment toward the CREB-binding protein [65]. Thus, it has been proposed that multisite phosphorylation acts as a rheostat to enhance binding of IDRs/IDPs to their partner. A similar binding mode could occur between GPCR-Cters and arrestin where multivalency of phosphates would enhance the affinity of GPCR to arrestin and stabilize the interaction [8,9].

Conclusions and outlook

Our study highlights a conformational transition between the basal non-phosphorylated state and the phosphomimetic state from transient helical or random coil to a β-strand conformation. This transition occurs in the region that interacts with arrestin-2. Moreover, no additional conformational changes were observed in the bound state of the variant of V2R-Cter, compared to its free state, suggesting that a conformational selection interaction mechanism could be involved. Based on this evidence, we hypothesize a model where GRK phosphorylation would dictate the final configuration of GPCR C-terminal domains to trigger the binding mode to arrestin. The selected arrestin conformation resulting from the interaction of GPCR phosphate with specific pockets of arrestin would expose specific interaction surfaces recognized by different cytosolic partners, and thus, modulate arrestin function. Hence, in this model, the signaling fate in the arrestin pathway would, at least in part, also depend on the structural impact of GRK-mediated phosphorylation has on its partners.

STAR*Methods

Key resource table

REAGENT or RESOURCE	SOURCE	IDENTIFIER
Bacterial and virus strains		
E. coli BL21(DE3) competent cells	ThermoFisher Scientific	Cat# EC0114
E. coli NiCo21(DE3) competent cells	NEB	Cat# C2529H
Chemicals, peptides, and recombinant proteins		
Complete® EDTA free protease inhibitor	Sigma-Aldrich	Cat# 4693132001
Alexa Fluor™ 350 maleimide	ThermoFisher	Cat# A30505
Alexa Fluor™ 488 maleimide	ThermoFisher	Cat# A10254
Recombinant DNA		
Genes : cDNA coding for pm-V2R (343–371), pm-GHSR (339–366), pm-b2AR (342–413) and cDNA coding for arrestin-2	Life technologies (GeneArt® gene synthesis)	N/A
Genes : cDNA coding for cysteine-free arrestin-2 mutant	Genecust	N/A
Plasmid : pETM33-(His)6-GST-3C-pm-GHSR	This paper	N/A
Plasmid : pETM33-(His)6-GST-3C-pm-V2	This paper	N/A
Plasmid : pET1a-(His)6-GST-TEV-pm-B2	This paper	N/A
Plasmid : pETM11-(His)6-TEV-arrestin-2	This paper	N/A
Plasmid : pET15B-(His)6-3C-cysfree-arrestin-2	This paper	N/A
Deposited data		
^{1}H, ^{15}N and ^{13}C NMR assignment of pm-V2R-Cter	BioMagResBank	BMRB : 51330
^{1}H, ^{15}N and ^{13}C NMR assignment of pm-GHSR-Cter	BioMagResBank	BMRB : 51328
^{1}H, ^{15}N and ^{13}C NMR assignment of pm-β2AR-Cter	BioMagResBank	BMRB : 51319
Software and algorithms		
ASTRA software	Wyatt	https://www.wyatt.com/products/software/astra.html
ATSAS software package	Manalastas-Cantos et al., 2021 Panjkovich and Svergun, 2018	https://www.embl-hamburg.de/biosaxs/software.html
NMRFAM-SPARKY	Lee et al., 2015	https://www.cgl.ucsf.edu/home/sparky/
Flexible-Meccano program	Ozenne et al., 2012b	https://www.ibs.fr/en/communication-outreach/scientific-output/software/flexible-meccano-en
FluorEssence V3.5	HORIBA Scientific	https://www.horiba.com/fra/scientific/products/detail/action/show/Product/fluoressence-1378/
MO.Affinity Analysis software	Nanotemper Technologies	https://shop.nanotemper tech.com/en/moaffinity-analysis-software-1-license-30
GraphPad Prism software	GraphPad Software Inc.	https://www.graphpad.com/features
FlexPepDock server	London et al., 2011	
RanCh program	Bernado et al., 2007	

PULCHRA program	Rotkiewicz and Skolnick, 2008	
DES-amber force field for Molecular-Dynamics simulation	Piana et al., 2020	https://github.com/paulrobustelli/Force-Fields
Gromacs 2020.5 tools	Abraham et al., 2015	https://manual.gromacs.org/documentation/2020.5/dev-manual/tools.html
LINCS algorithm	Hess et al., 1997	
Particle mesh Ewald tools	Darden et al., 1993	
Hoover thermostat	Nosé, 1984	

Resource Availability

Lead contact

Further information and requests for resources and reagents should be directed to and will be fulfilled by the lead contact, Nathalie Sibille (nathalie.sibille@cbs.cnrs.fr)

Materiel availability

All expression plasmids used in this study will be made available on request. This study did not generate new unique reagents.

Experimental model and subject details

The GPCR C-termini were expressed in BL21(DE3) E. coli cells grown in self-inducible medium N5052 (^{15}N labelling) or in minimal medium M9 (^{15}N and ^{13}C labelling). Arrestin-2 was expressed in BL21(DE3) E. coli cells grown in LB Broth media. Recombinant cysteine-free arrestin-2 was expressed in NiCo21(DE3) *E. coli* cells.

Methods details

Expression and purification

Recombinant human GPCR-Cter. Phosphomimetic GPCR C-termini genes were purchased from GeneArt gene synthesis (Life technologies). They were subcloned into pETM33 vector for GHSR-Cter and V2R-Cter and pET1a vector for β2AR-Cter. The constructs were fused with a $(His)_6$-GST-tagged followed by the HRV 3C protease recognition site (for GHSR-Cter and V2R-Cter) or by the TEV protease recognition site (for β2AR-Cter). The three GPCR C-termini were expressed and purified as described previously [27].

Recombinant rat arrestin-2. pETM11-arrestin-2 plasmid was transfected into *E. Coli* BL21 DE_3 strain (ThermoFisher Scientific). The cells were cultured and induced with 0.25 mM isopropyl-β-D-thiogalacoside (IPTG) at a OD_{600} of 0.5 nm. After growing over-night at 20 °C, bacteria were harvested, resuspended and lysed by French-Press. Cell debris was removed by centrifugation and the soluble fraction was loaded onto 5 mL HisTrap HP column (Cytiva) in buffer A (50 mM Tris pH 8, 200 mM NaCl and 2 mM DTT). The protein was recovered using step elution with buffer A supplemented with 500 mM imidazole. The eluted protein was dialyzed over night at 4 °C in buffer A with TEV protease (ratio protease:protein 1:50 (w/w)). Protease and His-TEV tag were removed using HisTrap HP column. Untagged proteins were diluted to 50 mM NaCl and injected into HiTrap Q HP (Cytiva) in buffer C (20

mM Tris pH 8, 50 mM NaCl and 2 mM DTT). The protein was eluted with a linear gradient of buffer C supplemented with 1M NaCl. Proteins were concentrated using a 10 kDa Millipore concentrator and injected into a HiLoad 16/60 Superdex 200 size exclusion column (Cytiva) in 50 mM Bis-Tris pH 6.7, 50 mM NaCl and 2 mM DTT. The purified proteins were then concentrated using Millipore concentrator and aliquots were flash-frozen in 50 mM Bis-Tris pH 6.7, 50 mM NaCl, 1 mM EDTA (EthyleneDiamineTetraAcetic acid), 0.5 mM TCEP (Tris(2-CarboxyEthyl)Phosphine) and stored at -80 °C.

Recombinant arrestin-2 for FRET experiments. The full-length cysteine-free arrestin-2 mutant was modified with two cysteines at positions 167 and 191 and an N-terminal hexahistidine tag followed by a 3C protease site. The sequence was codon-optimized for expression in *E. coli* and cloned into a pET-15b vector (Genecust). NiCo21(DE3) competent *E. coli* (NEB) cells were transformed with the resulting expression vector. Cultures were grown in 2YT medium supplemented with 100 µg/mL carbenicillin at 37°C up to an OD_{600} of 1.0. The temperature of the culture was then decreased to 16°C and protein synthesis induced with 25 µM IPTG for 20 hours. Cells were harvested and resuspended in ice-cold lysis buffer (50 mM Tris-HCl pH 8, 300 mM NaCl, 15% glycerol, 1 mM TCEP) supplemented with a protease inhibitor cocktail (Roche). Cells were lysed by sonication, centrifuged at 27,000xg for 45 minutes and the supernatant was applied to a HisTrap 5 mL column (GE Healtcare). The resin was washed with a 50 mM Tris-HCl pH 8, 300 mM NaCl, 15% glycerol, 1 mM TCEP buffer, with the same buffer supplemented with 20 mM imidazole then with the same buffer containing 40 mM imidazole. The protein was eluted with the same buffer containing 200 mM imidazole and dialyzed into a 25 mM Na-HEPES, 200 mM NaCl, 1 mM TCEP, 10% glycerol, pH 7.5 buffer. The protein after dialysis was digested with 3C protease at a protease:arrestin ratio of 1:10 (w:w) for 16 hours at 20 °C and subjected to reverse-nickel purification. The protein in the flow-through fractions were recovered, diluted with the same buffer devoid of NaCl to reach a final salt concentration of 40 mM and loaded on a HiSure Q 5 mL column (GE Healthcare). After washing with a 25 mM Na-HEPES, 40 mM NaCl, 1 mM TCEP, 10% glycerol, pH 7.5 buffer, elution was carried out with a linear 40 to 400 mM NaCl gradient in 25 mM Na-HEPES, 1 mM TCEP, 10% glycerol, pH 7.5. The fractions in the elution peak were pooled, concentrated using a 30 kDa spin concentrator (Amicon) and subjected to size-exclusion chromatography using a Superdex 200 increase 10/300 GL column (GE Healthcare) in a buffer 20 mM HEPES pH 7.5, 200 mM NaCl, 10% glycerol, 1 mM TCEP. The elution peak fractions were pooled and concentrated using a 30 kDa spin concentrator (Amicon) up to a concentration of 10-20 µM. A sequential labeling strategy was then used to label arrestin with the FRET probes [66]. Purified arrestin was first incubated with 0.8 equivalents of AlexaFluor350 maleimide (ThermoFisher) for 3 hours in the dark. Unreacted fluorophore was removed on a Zeba spin desalting column (ThermoFisher). 1.3 equivalents of AlexaFluor488 maleimide (ThermoFisher) were then added and incubated for 3 additional hours in the dark. The reaction was stopped with 5 mM L-cysteine and unreacted fluorophore again removed on a Zeba spin column (ThermoFisher). The degree of labeling was determined using the known extinction coefficients of the protein and both fluorophores at their absorbance maxima. The typical ratio of donor to arrestin was in the 0.8-0.9 range, with a typical acceptor/donor labeling ratio in the 1-1.2 range.

Biophysical characterization

Size Exclusion Chromatography – Multi-Angle Light Scattering (SEC-MALS). The experiments were performed at 25 °C using a Superdex 75 10/300 GL column (Cytiva) connected to a miniDAWN-TREOS light scattering detector and an Optilab T-rEX differential refractive index detector (Wyatt Technology, Santa Barbara, CA). The column was equilibrated in 50 mM BisTris pH 6.7, 50 mM NaCl, 1 mM TCEP and 0.5 mM EDTA buffer filtered at 0.1 µM, and the SEC-MALS system was calibrated with a sample of Bovine Serum Albumin (BSA) at 1 mg/mL. Samples were prepared at 1.16 mM, 1.30 mM and 0.35 mM for pm-V2R-Cter, pm-GHSR-Cter and pm-β2AR-Cter, respectively. For each GPCR-Cter, 40 µL of sample were injected at 0.5 mL/min. Data acquisition and analyses were performed using the ASTRA software (Wyatt).

***Circular Dichroism (CD) spectroscopy*.** Far UV-spectra of the three pm-GPCR-Cters were recorded in a quartz cuvette (path length 0.1 cm) at 0.08 mg/mL in H_2O at 20 °C using a Chirascan. The ellipticity was scanned from 190 to 260 nm with an increment of 0.5 nm, an integration time of 3 s, and a constant band-pass of 1 nm. Data were treated using Chirascan and, after subtraction of the buffer signal, were converted to mean residue ellipticity ($[\theta]_{MRW}$, mdeg.cm².dmole^{-1}) using equation (1) [67]:

$$(1) \quad [\theta]_{\mathrm{MWR}} = [(\theta \text{ x } \mathrm{Mw})/(\mathrm{L} \text{ x } \mathrm{C} \text{ x } 10)]/(\mathrm{n}-1)$$

where θ is the ellipticity (mdeg), Mw is the molecular weight (g/mol), L is the cuve lengh (cm), C is the protein concentration (mg/mL) and n is the number of peptid bond.

Small-angle X-ray scattering (SAXS) measurement and analysis. Synchrotron radiation small-angle X-ray scattering (SAXS) data were acquired for pm-GPCR-Cters at the SWING beamline at the SOLEIL synchrotron (Saint-Aubin, France) [68] using an X-ray wavelength of 1.03 Å and a sample-to-detector distance of 2.00 m. Samples were measured at 15 °C and at two concentrations, 5 mg/mL and 10 mg/mL, for all GPCR-Cters, in 50 mM BisTris pH 6.7, 50 mM NaCl and 2 mM DTT buffer. Before exposure to X-rays, 45 µl of sample were injected into 3 mL Superdex 75 5/150 GL column (Cytiva) at 0.2 mL/min, pre-equilibrated into the same buffer as samples. The intensity was measured as function of the magnitude of the scattering vector, s, using equation (2) [69]:

$$(2) \quad s = 4\pi.\sin(\theta)/\lambda$$

where θ the scattering angle and λ the X-ray wavelength.

The scattering patterns of the buffer were recorded before the void volume of the column (1 mL). The scattering profiles measured covered a momentum transfer range of $0.002 < s < 0.5$ Å^{-1}. Data were processed using CHROMIX from ATSAS software package to select automatically frames corresponding to buffer and sample, and perform buffer subtraction [70]. The scaled and averaged SAXS curves were analyzed using Primus from ATSAS software package. AUTORG was used to calculate the radius of gyration.

Nuclear Magnetic Resonance (NMR) spectroscopy

All NMR experiments were performed on Bruker Avance III 700 MHz, except 3D assignment experiments of β2AR-Cter and chemical shift perturbation (CSP) experiments at 800 MHz. The spectrometers are equipped with a cryogenic triple-resonance (^{1}H, ^{15}N, ^{13}C) probe and shielded z-

gradients. All NMR experiments were recorded, unless otherwise stated, at 20 °C in a buffer (named NMR buffer) composed of 50 mM Bis-Tris pH 6.7, 150 mM NaCl, 1 mM EDTA, 0.5 mM TCEP, 5 % D_2O (Eurisotop) and 5 mM DSS-d6 (2,2-dimethyl-2-silapentane-5-sulfonate, Sigma) as internal reference [71]. All experiments used the pulse sequences provided by Bruker Topspin 3.2. Squared cosine apodization was used in indirect dimensions, prior to zero-filling and Fourier transformation using TOPSPIN (version 4.0.6, Bruker) and data processing was performed using NMRFAM-SPARKY (version 1.414, [72]). For each NMR experiments, except CSP, concentrations of pm-GPCR-Cters were indicated in Table S1.

Backbone assignment. For the sequential backbone assignment of the $^{13}C/^{15}N$ labeled pm-V2R-Cter, pm-GHSR-Cter and pm-β2AR-Cter, HNCO, HN(CA)CO, HNCA, HN(CO)CA, CBCA(CO)NH and HNCACB triple resonance 3D experiments were recorded. H_N, N, CO, C_α and C_β nuclei of all residues were assigned, expected the first glycine N-terminal residue, the residue A339 of β2AR-Cter and proline residues.

Secondary Chemical Shift (SCS). $^{13}C_\alpha$ and $^{13}C_\beta$ chemical shifts were used to calculate SCS by subtraction of experimental chemical shifts (from the 3D experiment) from random-coil chemical shift calculated by POTENCI database [48,49]. To calculate SCS for interaction experiments, HNCACB triple resonance 3D experiments were recorded on a sample of 50 µM $^{13}C/^{15}N$ labeled pm-V2R-Cter free and in presence of 250 µM of arrestin-2 in a NMR buffer at 50 mM NaCl.

$^3J_{HNHA}$ scalar coupling. $^3J_{HNHA}$ scalar coupling measurements were obtain accordingly to Vuister and Bax [73]. HNHA experiments were recorded in NMR buffer ^{15}N-labeled pm-GPCR-Cter. Intensity of the cross-peak (S_{cross}) and intensity of the corresponding diagonal peak (S_{diag}) were extracted using Sparky. They were used to calculate the $^3J_{HNHA}$ scalar coupling of each amino acid using the equation (3):

$$(3) \quad S_{cross}/S_{diag} = -tan^2\,(2\xi\pi\,.\,{}^3J_{HNHA})$$

Where 2ξ is the total evolution time for the homonuclear $^3J_{HNHA}$ coupling, which has been set to 26.1 ms.

^{15}N NMR relaxation experiments. Relaxation data were recorded on ^{15}N-labeled pm-GPCR-Cter. Heteronuclear $^{15}N\{^1H\}$-NOE values were determined from two experiments with on- (saturated spectrum) and off-resonance ^1H saturation (unsaturated spectrum) which were recorded in an interleaved manner. The saturation time by 120° pulses (~ 10 kHz) was set to 6 s and the recycle delay to 6 s. NOEs values were obtained from the ratio of intensities measured in the saturated (I) and unsaturated (I_0) spectra. Longitudinal (R_1) and transversal (R_2) relaxation rate were measured through acquisition of ^{15}N-HSQC spectra with different relaxation delays: 10, 50, 100, 200, 400, 600, 800, 1 000 ms for R_1, and 16, 32, 64, 96, 160, 240, 480, 640 ms for R_2. For each pick, intensity was fitted to a single exponential decay using Sparky [72] to obtain the relaxation parameters. For all relaxation parameters, three residues at N- and C-extremity were discarded from the calculation of average values due to their inherent higher flexibility.

^1H-^{15}N Residual Dipolar Coupling (RDC). Residual dipolar couplings were recorded on ^{15}N-labeled pm-GPCR-Cter using 2D IPAP HSQC spectra [74] in isotropic and anisotropic media. For the anisotropic media, the samples were dissolved in a liquid-crystalline medium composed by 5 % (w/v) mixture of 0.85 molar ratio of polyoxyethylene 5-lauryl ether (PEG/$C_{12}E_5$) (Sigma) and 1-hexanol (Sigma) [75] or in ~ 20 mg/mL of filamentous phage Pf1 (Asla biotech) [76]. For pm-V2R-Cter and pm-β2AR-Cter (Fig. S5b), we analyzed RDCs in alcohol mixture (quadrupolar splitting of 33 Hz and 36 Hz, respectively), for pm-

GHSR-Cter, in Pf1 medium with a quadrupolar splitting of 15.2 Hz. For more details see previous Material and Methods [27]. The $^{1}D_{NH}$ coupling constants were obtained from the relative peak positions in the ^{15}N dimension measured in the *sum* and *diff* subspectra (upfield and downfield components of the doublet).

Paramagnetic Relaxation Enhancement (PRE). The C378A or C406A variants of ^{15}N-pm-β2AR-Cter were labeled on the remaining cysteine using 3-(2-Iodoacetamido)-proxyl (Merck). Paramagnetic samples were recorded with a recycling delay of 2 s. Reference diamagnetic samples were recorded in the same condition after addition of 5 mM fresh ascorbic acid, pH 6.7, in the NMR tube. PRE were analyzed by measuring the peak intensity ratios (I_{para}/I_{dia}) between two ^{15}N-HSQC spectra of paramagnetic and diamagnetic samples, and the theoretical profile was calculated as in a strictly random coil polymer [77].

Chemical Shift Perturbation (CSP). The interaction between ^{15}N-labeled GPCR C-termini and the unlabeled arrestin-2 was measured in NMR buffer containing 50 mM NaCl in order to limit the screening of potential electrostatic interactions. ^{15}N-HSQC spectra were recorded on the 800 MHz spectrometer at 1:0, 1:1, 1:2, 1:5 and 1:10 ^{15}N-GPCR-Cter:arrestin-2 ratio. At each point of the titration and before to record the spectrum, the complex is incubated 30 min at room temperature. For each peak in ^{15}N-HSQC spectra, the intensity ratio (I/I_{REF}) is calculated between the bound (I) and free states (I_{REF}). Means of intensity ratio subtracted with the mean of uncertainty value was chosen as cut-off values, by excluding residues in interaction. Chemical shift perturbation Δδ were calculated using equation (4) [78]:

$$(4) \quad \Delta\delta = [0.5((\Delta H)^2 + (\Delta N/5)^2)]^{1/2}$$

Where Δδ is the chemical shift perturbation (in ppm), ΔH is the subtraction of ^{1}H chemical shift in the bound and free state and ΔN is the subtraction of ^{15}N chemical shift in the bound and free state. The overlapped residues in HSQC spectra were removed for the chemical shift perturbation calculation. Standard deviation multiplied by 4 was chosen as cut-off values [45]. Residues in interaction were removed from standard deviation calculation.

Ensemble Calculations. Ensembles of explicit models were generated using Flexible-Meccano (FM) [79], which sequentially builds peptide planes based on amino acid specific conformational propensity and a simple volume exclusion term. To account for deviations from a random-coil description, different structure ensembles of 50,000 conformers were computed including user-defined local conformational propensities in different regions of the protein. Local conformational propensities were first localized using the consensus of all NMR data, and then were adjusted by comparing back-calculated and experimental $^{1}D_{HN}$ RDCs to get the lowest X^2 (for more details [41]). For pm-β2AR-Cter, as for pm-β2AR-Cter [41], a long-range contact of 15 Å between two regions affected by the probe, i.e., from residues 338 to 357 and from residues 367 to 386 (regions in grey in Fig. S5), was introduced to get a better agreement between back-calculated and experimental $^{1}D_{HN}$ RDCs.

FRET measurements

Fluorescence spectra were recorded on a Fluoromax-4 TCSP spectrofluorimeter (Horiba). Protein concentrations in the 0.5 µM range were used. Fluorescence emission spectra were recorded at 20 °C between 400 nm and 600 nm (λ_{exc} 343 nm) or 510 and 600 nm (λ_{exc} 500 nm) with 5 nm excitation and

emission slits and 0.5 nm intervals. The absence of The FRET ratio corresponds to the ratio of the acceptor emitted fluorescence at 520 nm following excitation at two different wavelengths, 345 and 500 nm. FRET changes were calculated using the values obtained for arrestin in the presence of an irrelevant peptide as a reference and were expressed as %. Removal of acceptor bleedthrough and correction of direct acceptor excitation were carried out as described previously [80].

Dissociation constant estimation

Microscale thermophoresis (MST). Arrestin-2 was buffer-exchanged by using PD MiniTrap™ G-10 (Cytiva), in 50 mM Bis-Tris pH 7.5, 50 mM NaCl and 1 mM TCEP labeling buffer. Alexa Fluor® 488 Maleimide C5 (ThermoFisher Scientific) dye was added in 10-fold molar excess in 250 µL at 7 µM of arrestin-2. After 1 h at 4 °C, the reaction was quenched by adding 100 mM of L-cysteine and incubates during 15 min at room temperature. Buffer was exchanged and the free dye removed by gravity gel filtration using PD MiniTrap™ G-10 (Cytiva) into 50 mM HEPES pH 7.5, 50 mM NaCl. The labeling efficiency was calculated using absorbance at 280 nm (ε_{280} = 19,370 $M^{-1}.cm^{-1}$) for arrestin-2 and 495 nm (ε_{495} = 71,000 $M^{-1}.cm^{-1}$) for the dye. A correction factor of 0.11 was assumed for the absorbance at 495 nm to compensate the dye's absorbance at 280 nm. After incubation of 5 nM of arrestin-2 labeled with an increasing amount of pm-GHSR-Cter (0.01-450 µM) at 20 °C during 30 min, sample were loaded into standard capillaries (Monolith NT Capillaries, Nanotemper Technologies). Before each measurement, all samples were centrifuged at 12,000 g during 15 min. Measurement was performed on a Monolith NT.115 MST apparatus (NanoTemper Technologies), by using a range excitation wavelength between 460 and 480 nm and a range emission wavelength measured between 515 and 530 nm. Dose-response curve was plotted using the MO.Affinity Analysis software (Nanotemper Technologies) and outlier values were removed. One-site binding model was used to calculate the K_d value.

Fluorescence anisotropy. pm-GHSR-Cter was buffer-exchanged by using PD MiniTrap™ G-10 (Cytiva), in labeling buffer (50 mM Bis-Tris pH 7, 50 mM NaCl and 1 mM TCEP). Alexa Fluor® 488 succinimidyl ester (ThermoFisher) was added in 10-fold molar excess in 100 µL at 50 µM of pm-GHSR-Cter. After an incubation of 1 h at room temperature, protected from light and under gentle agitation, the reaction was stopped by adding 10 µL of 1 M Tris and incubated for 15 min. Buffer was exchanged and the free dye removed by gravity gel filtration using PD MiniTrap™ G-10 (Cytiva) into labeling buffer. The labeling efficiency was calculated using absorbance at 280 nm (ε_{280} = 5500 $M^{-1}.cm^{-1}$) for pm-GHSR-Cter and 495 nm (ε_{495} = 71 000 $M^{-1}.cm^{-1}$) for the dye. A correction factor of 0.11 was assumed for the absorbance at 495 nm to compensate the dye's absorbance at 280 nm. After 30 min incubation of 1 nM of pm-GHSR-Cter with increasing amounts of arrestin-2 (0-670 µM), samples were centrifuged at 12,000 g during 15 min. Measurement of fluorescence anisotropy was performed using a Tecan Safire II micro plate reader fluorescence spectrometer and a Corning 384 Low Flange Black Flat Bottom plate. Excitation and emission wavelengths were respectively measured at 470 nm and 530 nm. K_D value was calculated by nonlinear regression analysis using a sigmoid curve fit from GraphPad Software

Modeling of GPCR-Cter:Arrestin complexes

The complexes of GPCR-Cters and arrestin-2 were modeled using the following steps. First, the stretch of residues identified to be involved in binding based on NMR data was modeled in complex with arrestin-2 using the crystal structure of V2Rpp in complex with arrestin-2 (PDB ID: 4JQI). This included residues 356-364 for V2 and 360-367 for GHSR. These models were then refined using FlexPepDock server (**PMID: 21622962, 20455260**). The rest of the residues of Cters were added using the program RanCh [81,82] followed by addition of backbone and side-chain atoms using PULCHRA (**PMID: 18196502**). These structures were then subjected to Molecular Dynamics (MD) simulations using the DES-amber force field (doi: 10.1021/acs.jctc.9b00251) obtained from https://github.com/paulrobustelli/Force-Fields. The simulation system was prepared using the tools available with gromacs 2020.5. This included addition of hydrogens, solvating in a box of TIP4P-D water molecules, neutralizing the system with the associated Na^+ and Cl^- ions with scaled charges and setting the salt concentration to 0.15 M. We used periodic boundary conditions and restrained the bonds involving hydrogen atoms using LINCS algorithm [83]. The electrostatic interactions were calculated using particle mesh Ewald (PME) [84] with a cutoff of 9 Å for long-range interactions. The system was minimized for 10,000 steps using steepest descent algorithm followed by NVT (constant number, volume and temperature) equilibration in 3 steps. In the first step, all the backbone atoms were restrained using a force constant of 1000 kJ/mol.nm^2. In the second step, the region of Cters refined using FlexPepDock and the residues of arrestin-2 within 5 Å of this region were kept restrained while the rest of the proteins were allowed to move freely for 20 ns. In the third step, only the short region of the Cters, which forms beta-sheet, was restrained and the system was equilibrated for 20 ns. Finally, all the restraints were released and the 4 independent NPT (constant number, pressure and temperature) simulations of 250 ns each were carried out accumulating 1 μs of unrestrained simulations for each Cter. The temperature was maintained at 303.15 K using a Nose-Hoover thermostat [85] and for NPT simulations, the pressure was maintained at 1 bar using Parrinello-Rahman barostat [86].

Quantification and statistical analysis

Statistical analyses for NMR data were performed using NMRFAM-SPARKY (version 1.414). Data are expressed as the mean ± SD.

Statistical analyses for fluorescence anisotropy were performed using GraphPad Prism (GraphPad Software Inc.). Data are expressed as the mean ± SD.

References

1. Ahn, S., Shenoy, S.K., Luttrell, L.M., and Lefkowitz, R.J. (2020). SnapShot: β-Arrestin Functions. Cell *182*, 1362-1362.e1. 10.1016/j.cell.2020.07.034.
2. Tobin, A.B., Butcher, A.J., and Kong, K.C. (2008). Location, location, location...site-specific GPCR phosphorylation offers a mechanism for cell-type-specific signalling. Trends Pharmacol Sci *29*, 413–420. 10.1016/j.tips.2008.05.006.
3. Kim, J., Ahn, S., Ren, X.-R., Whalen, E.J., Reiter, E., Wei, H., and Lefkowitz, R.J. (2004). Functional antagonism of different G protein-coupled receptor kinases for-arrestin-mediated angiotensin II receptor signaling.
4. Nobles, K.N., Xiao, K., Ahn, S., Shukla, A.K., Lam, C.M., Rajagopal, S., Strachan, R.T., Huang, T.Y., Bressler, E.A., Hara, M.R., et al. (2011). Distinct phosphorylation sites on

the beta(2)-adrenergic receptor establish a barcode that encodes differential functions of beta-arrestin. Sci Signal *4*, ra51. 10.1126/scisignal.2001707.

5. Pals-Rylaarsdam, R., Xu, Y., Witt-Enderby, P., Benovic, J.L., and Hosey, M.M. (1995). Desensitization and internalization of the m2 muscarinic acetylcholine receptor are directed by independent mechanisms. Journal of Biological Chemistry *270*, 29004–29011. 10.1074/jbc.270.48.29004.
6. Pals-Rylaarsdam, R., Gurevich, V. V., Lee, K.B., Ptasienski, J.A., Benovic, J.L., and Hosey, M.M. (1997). Internalization of the m2 muscarinic acetylcholine receptor. Arrestin-independent and -dependent pathways. Journal of Biological Chemistry *272*, 23682–23689. 10.1074/jbc.272.38.23682.
7. Staus, D.P., Hu, H., Robertson, M.J., Kleinhenz, A.L.W., Wingler, L.M., Capel, W.D., Latorraca, N.R., Lefkowitz, R.J., and Skiniotis, G. (2020). Structure of the M2 muscarinic receptor-beta-arrestin complex in a lipid nanodisc. Nature *579*, 297–302. 10.1038/s41586-020-1954-0.
8. Zhou, X.E., He, Y., de Waal, P.W., Gao, X., Kang, Y., Van Eps, N., Yin, Y., Pal, K., Goswami, D., White, T.A., et al. (2017). Identification of Phosphorylation Codes for Arrestin Recruitment by G Protein-Coupled Receptors. Cell *170*, 457-469.e13. 10.1016/j.cell.2017.07.002.
9. He, Q.-T., Xiao, P., Huang, S.-M., Jia, Y.-L., Zhu, Z.-L., Lin, J.-Y., Yang, F., Tao, X.-N., Zhao, R.-J., Gao, F.-Y., et al. (2021). Structural studies of phosphorylation-dependent interactions between the V2R receptor and arrestin-2. Nat Commun *12*, 2396. 10.1038/s41467-021-22731-x.
10. Huang, W., Masureel, M., Qu, Q., Janetzko, J., Inoue, A., Kato, H.E., Robertson, M.J., Nguyen, K.C., Glenn, J.S., Skiniotis, G., et al. (2020). Structure of the neurotensin receptor 1 in complex with beta-arrestin 1. Nature *579*, 303–308. 10.1038/s41586-020-1953-1.
11. Ren, X.-R., Reiter, E., Ahn, S., Kim, J., Chen, W., and Lefkowitz, R.J. (2004). Different G protein-coupled receptor kinases govern G protein and-arrestin-mediated signaling of V2 vasopressin receptor.
12. Choi, M., Staus, D.P., Wingler, L.M., Ahn, S., Pani, B., Capel, W.D., and Lefkowitz, R.J. (2018). G protein-coupled receptor kinases (GRKs) orchestrate biased agonism at the β 2-adrenergic receptor.
13. Kaya, A.I., Perry, N.A., Gurevich, V. V, and Iverson, T.M. Phosphorylation barcode-dependent signal bias of the dopamine D1 receptor. 10.1073/pnas.1918736117/-/DCSupplemental.
14. Maharana, J., Sarma, P., Yadav, M.K., Saha, S., Singh, V., Saha, S., Chami, M., Banerjee, R., and Shukla, A.K. (2023). Structural snapshots uncover a key phosphorylation motif in GPCRs driving β-arrestin activation. Mol Cell *83*, 2091-2107.e7. 10.1016/j.molcel.2023.04.025.

15. He, Q.-T., Xiao, P., Huang, S.-M., Jia, Y.-L., Zhu, Z.-L., Lin, J.-Y., Yang, F., Tao, X.-N., Zhao, R.-J., Gao, F.-Y., et al. (2021). Structural studies of phosphorylation-dependent interactions between the V2R receptor and arrestin-2. Nat Commun *12*, 2396. 10.1038/s41467-021-22731-x.
16. Min, K., Yoon, H.-J., Park, J.Y., Baidya, M., Dwivedi-Agnihotri, H., Maharana, J., Chaturvedi, M., Chung, K.Y., Shukla, A.K., and Lee, H.H. (2020). Crystal Structure of β-Arrestin 2 in Complex with CXCR7 Phosphopeptide. Structure. 10.1016/j.str.2020.06.002.
17. Lee, Y., Warne, T., Nehmé, R., Pandey, S., Dwivedi-Agnihotri, H., Chaturvedi, M., Edwards, P.C., García-Nafría, J., Leslie, A.G.W., Shukla, A.K., et al. (2020). Molecular basis of β-arrestin coupling to formoterol-bound β1-adrenoceptor. Nature *583*, 862–866. 10.1038/s41586-020-2419-1.
18. Yin, W., Li, Z., Jin, M., Yin, Y.L., de Waal, P.W., Pal, K., Yin, Y., Gao, X., He, Y., Gao, J., et al. (2019). A complex structure of arrestin-2 bound to a G protein-coupled receptor. Cell Res *29*, 971–983. 10.1038/s41422-019-0256-2.
19. Bous, J., Fouillen, A., Orcel, H., Trapani, S., Cong, X., Fontanel, S., Saint-Paul, J., Lai-Kee-Him, J., Urbach, S., Sibille, N., et al. (2022). Structure of the vasopressin hormone-V2 receptor-β-arrestin1 ternary complex.
20. Guillien, M., le Maire, A., Mouhand, A., Bernadó, P., Bourguet, W., Banères, J.L., and Sibille, N. (2020). IDPs and their complexes in GPCR and nuclear receptor signaling 1st ed. (Elsevier Inc.) 10.1016/bs.pmbts.2020.05.001.
21. Uversky, V.N., Gillespie, J.R., and Fink, A.L. (2000). Why are “natively unfolded” proteins unstructured under physiologic conditions? Proteins: Structure, Function and Genetics *41*, 415–427. 10.1002/1097-0134(20001115)41:3<415::AID-PROT130>3.0.CO;2-7.
22. Dunker, A.K., Lawson, J.D., Brown, C.J., Williams, R.M., Romero, P., Oh, J.S., Oldfield, C.J., Campen, A.M., Ratliff, C.M., Hipps, K.W., et al. (2001). Intrinsically disordered protein. J Mol Graph Model *19*, 26–59. https://doi.org/10.1016/S1093-3263(00)00138-8.
23. Zhou, J., Zhao, S., and Dunker, A.K. (2018). Intrinsically Disordered Proteins Link Alternative Splicing and Post-translational Modifications to Complex Cell Signaling and Regulation. J Mol Biol *430*, 2342–2359. 10.1016/j.jmb.2018.03.028.
24. Wright, P.E., and Dyson, H.J. (2015). Intrinsically disordered proteins in cellular signalling and regulation. Nat Rev Mol Cell Biol *16*, 18–29. 10.1038/nrm3920.
25. Kriwacki, R.W., Hengst, L., Tennant, L., Reed, S.I., and Wright, P.E. (1996). Structural studies of p2 lWa1CiPl / Sdil in the free and Cdk2-bound state : Conformational disorder mediates binding diversity. *93*, 11504–11509.
26. Olsen, J.G., Teilum, K., and Kragelund, B.B. (2017). Behaviour of intrinsically disordered proteins in protein–protein complexes with an emphasis on fuzziness. Cellular and Molecular Life Sciences *74*, 3175–3183. 10.1007/s00018-017-2560-7.
27. Guillien, M., Mouhand, A., Fournet, A., Gontier, A., Thureau, A., Allemand, F., Banères, J.-L., Bernadó, P., and Sibille, N. (2022). Structural insights into the intrinsically

disordered GPCR C-terminal region, major actor in arrestin-GPCR interaction. Biomolecules.

28. Nobles, K.N., Guan, Z., Xiao, K., Oas, T.G., and Lefkowitz, R.J. (2007). The active conformation of beta-arrestin1: direct evidence for the phosphate sensor in the N-domain and conformational differences in the active states of beta-arrestins1 and -2. J Biol Chem *282*, 21370–21381. 10.1074/jbc.M611483200.
29. Bouzo-Lorenzo, M., Santo-Zas, I., Lodeiro, M., Nogueiras, R., Casanueva, F.F., Castro, M., Pazos, Y., Tobin, A.B., Butcher, A.J., and Camina, J.P. (2016). Distinct phosphorylation sites on the ghrelin receptor, GHSR1a, establish a code that determines the functions of ss-arrestins. Sci Rep *6*, 22495. 10.1038/srep22495.
30. Pearlman, S.M., Serber, Z., and Ferrell, J.E. (2011). A Mechanism for the Evolution of Phosphorylation Sites. Cell *147*, 934–946. 10.1016/j.cell.2011.08.052.
31. Bibow, S., Ozenne, V., Biernat, J., Blackledge, M., Mandelkow, E., and Zweckstetter, M. (2011). Structural impact of proline-directed pseudophosphorylation at AT8, AT100, and PHF1 epitopes on 441-residue tau. J Am Chem Soc *133*, 15842–15845. 10.1021/ja205836j.
32. Fischer, D., Mukrasch, M.D., Biernat, J., Bibow, S., Blackledge, M., Griesinger, C., Mandelkow, E., and Zweckstetter, M. (2009). Conformational changes specific for pseudophosphorylation at serine 262 selectively impair binding of tau to microtubules. Biochemistry *48*, 10047–10055. 10.1021/bi901090m.
33. Oakley, R.H., Laporte, S.A., Holt, J.A., Caron, M.G., and Barak, L.S. (2000). Differential Affinities of Visual Arrestin, βArrestin1, and βArrestin2 for G Protein-coupled Receptors Delineate Two Major Classes of Receptors. Journal of Biological Chemistry *275*, 17201–17210. 10.1074/jbc.M910348199.
34. Bouzo-Lorenzo, M., Santo-Zas, I., Lodeiro, M., Nogueiras, R., Casanueva, F.F., Castro, M., Pazos, Y., Tobin, A.B., Butcher, A.J., and Camina, J.P. (2016). Distinct phosphorylation sites on the ghrelin receptor, GHSR1a, establish a code that determines the functions of ss-arrestins. Sci Rep *6*, 22495. 10.1038/srep22495.
35. Bous, J., Orcel, H., Floquet, N., Leyrat, C., Lai-Kee-Him, J., Gaibelet, G., Ancelin, A., Saint-Paul, J., Trapani, S., Louet, M., et al. (2021). Cryo–electron microscopy structure of the antidiuretic hormone arginine-vasopressin V2 receptor signaling complex. Sci Adv *7*, 1–18. 10.1126/sciadv.abg5628.
36. Uversky, V.N. (2012). Size-Exclusion Chromatography in Structural Analysis of Intrinsically Disordered Proteins. In Intrinsically Disordered Protein Analysis: Volume 2, Methods and Experimental Tools Methods in Molecular Biology., V. N. Uversky and A. K. Dunker, eds. (Springer), pp. 179–194.
37. Woody, R.W. (1996). Theory of Circular Dichroism of Proteins. In Circular Dichroism and the Conformational Analysis of Biomolecules, G. D. Fasman, ed. (Springer US), pp. 25–67.

38. Sibille, N., and Bernadó, P. (2012). Structural characterization of intrinsically disordered proteins by the combined use of NMR and SAXS. Biochem Soc Trans *40*, 955–962. 10.1042/BST20120149.
39. Cordeiro, T.N., Herranz-Trillo, F., Urbanek, A., Estaña, A., Cortés, J., Sibille, N., and Bernadó, P. (2017). Structural characterization of highly flexible proteins by small-angle scattering. In Advances in Experimental Medicine and Biology (Springer New York LLC), pp. 107–129. 10.1007/978-981-10-6038-0_7.
40. Cordeiro, T.N., Herranz-Trillo, F., Urbanek, A., Estaña, A., Cortés, J., Sibille, N., and Bernadó, P. (2017). Small-angle scattering studies of intrinsically disordered proteins and their complexes. Curr Opin Struct Biol *42*, 15–23. 10.1016/j.sbi.2016.10.011.
41. Senicourt, L., le Maire, A., Allemand, F., Carvalho, J.E., Guee, L., Germain, P., Schubert, M., Bernadó, P., Bourguet, W., and Sibille, N. (2021). Structural insights into the interaction of the intrinsically disordered co-activator TIF2 with retinoic acid receptor heterodimer (RXR/RAR). J Mol Biol, 166899. https://doi.org/10.1016/j.jmb.2021.166899.
42. Bernadó, P., Blanchard, L., Timmins, P., Marion, D., Ruigrok, R.W.H., and Blackledge, M. (2005). A structural model for unfolded proteins from residual dipolar couplings and small-angle x-ray scattering. Proc Natl Acad Sci U S A *102*, 17002–17007. 10.1073/pnas.0506202102.
43. Ozenne, V., Bauer, F., Salmon, L., Huang, J. -r., Jensen, M.R., Segard, S., Bernado, P., Charavay, C., and Blackledge, M. (2012). Flexible-meccano: a tool for the generation of explicit ensemble descriptions of intrinsically disordered proteins and their associated experimental observables. Bioinformatics *28*, 1463–1470. 10.1093/bioinformatics/bts172.
44. Schumann, F.H., Riepl, H., Maurer, T., Gronwald, W., Neidig, K.-P., and Kalbitzer, H.R. (2007). Combined chemical shift changes and amino acid specific chemical shift mapping of protein-protein interactions. J Biomol NMR *39*, 275–289. 10.1007/s10858-007-9197-z.
45. Williamson, M.P. (2013). Using chemical shift perturbation to characterise ligand binding. Prog Nucl Magn Reson Spectrosc *73*, 1–16. 10.1016/j.pnmrs.2013.02.001.
46. Hornbeck, P. V, Zhang, B., Murray, B., Kornhauser, J.M., Latham, V., and Skrzypek, E. (2015). PhosphoSitePlus, 2014: mutations, PTMs and recalibrations. Nucleic Acids Res *43*, D512-520. 10.1093/nar/gku1267.
47. Oakley, R.H., Laporte, S.A., Holt, J.A., Caron, M.G., and Barak, L.S. (2000). Differential Affinities of Visual Arrestin, βArrestin1, and βArrestin2 for G Protein-coupled Receptors Delineate Two Major Classes of Receptors. Journal of Biological Chemistry *275*, 17201–17210. 10.1074/jbc.M910348199.
48. Tamiola, K., Acar, B., and Mulder, F. a a (2010). Sequence-specific random coil chemical shifts of intrinsically disordered proteins. J Am Chem Soc *132*, 18000–18003. 10.1021/ja105656t.

49. Nielsen, J.T., and Mulder, F.A.A. (2018). POTENCI: prediction of temperature, neighbor and pH-corrected chemical shifts for intrinsically disordered proteins. J Biomol NMR *70*, 141–165. 10.1007/s10858-018-0166-5.

50. Han, M.J., He, Q.T., Yang, M., Chen, C., Yao, Y., Liu, X., Wang, Y., Zhu, Z.L., Zhu, K.K., Qu, C., et al. (2021). Single-molecule FRET and conformational analysis of beta-arrestin-1 through genetic code expansion and a Se-click reaction. Chem Sci *12*, 9114–9123. 10.1039/d1sc02653d.

51. Isaikina, P., Petrovic, I., Jakob, R.P., Sarma, P., Ranjan, A., Baruah, M., Panwalkar, V., Maier, T., Shukla, A.K., and Grzesiek, S. (2023). A key GPCR phosphorylation motif discovered in arrestin2·CCR5 phosphopeptide complexes. Mol Cell *83*, 2108-2121.e7. 10.1016/j.molcel.2023.05.002.

52. Shukla, A.K., Manglik, A., Kruse, A.C., Xiao, K., Reis, R.I., Tseng, W.C., Staus, D.P., Hilger, D., Uysal, S., Huang, L.Y., et al. (2013). Structure of active β-arrestin-1 bound to a G-protein-coupled receptor phosphopeptide. Nature *497*, 137–141. 10.1038/nature12120.

53. Baidya, M., Kumari, P., Dwivedi-Agnihotri, H., Pandey, S., Chaturvedi, M., Stepniewski, T.M., Kawakami, K., Cao, Y., Laporte, S.A., Selent, J., et al. (2020). Key phosphorylation sites in GPCR s orchestrate the contribution of β-Arrestin 1 in ERK 1/2 activation . EMBO Rep *21*, 1–17. 10.15252/embr.201949886.

54. Kang, Y., Zhou, X.E., Gao, X., He, Y., Liu, W., Ishchenko, A., Barty, A., White, T.A., Yefanov, O., Han, G.W., et al. (2015). Crystal structure of rhodopsin bound to arrestin by femtosecond X-ray laser. Nature *523*, 561–567. 10.1038/nature14656.

55. Xie, H., Vucetic, S., Iakoucheva, L.M., Oldfield, C.J., Dunker, A.K., Uversky, V.N., and Obradovic, Z. (2007). Functional Anthology of Intrinsic Disorder. 1. Biological Processes and Functions of Proteins with Long Disordered Regions. J Proteome Res *6*, 1882–1898. 10.1021/pr060392u.

56. Cordeiro, T.N., Sibille, N., Germain, P., Barthe, P., Boulahtouf, A., Allemand, F., Bailly, R., Vivat, V., Ebel, C., Barducci, A., et al. (2019). Interplay of Protein Disorder in Retinoic Acid Receptor Heterodimer and Its Corepressor Regulates Gene Expression. Structure *27*, 1270–1285. 10.1016/j.str.2019.05.001.

57. Gurevich, V. V, and Gurevich, E. V (2019). GPCR Signaling Regulation: The Role of GRKs and Arrestins. Front Pharmacol *10*, 125. 10.3389/fphar.2019.00125.

58. Mayer, D., Damberger, F.F., Samarasimhareddy, M., Feldmueller, M., Vuckovic, Z., Flock, T., Bauer, B., Mutt, E., Zosel, F., Allain, F.H.T., et al. (2019). Distinct G protein-coupled receptor phosphorylation motifs modulate arrestin affinity and activation and global conformation. Nat Commun *10*, 1–14. 10.1038/s41467-019-09204-y.

59. Bah, A., Vernon, R.M., Siddiqui, Z., Krzeminski, M., Muhandiram, R., Zhao, C., Sonenberg, N., Kay, L.E., and Forman-Kay, J.D. (2015). Folding of an intrinsically disordered protein by phosphorylation as a regulatory switch. Nature. 10.1038/nature13999.

60. Shukla, A.K., Manglik, A., Kruse, A.C., Xiao, K., Reis, R.I., Tseng, W.C., Staus, D.P., Hilger, D., Uysal, S., Huang, L.Y., et al. (2013). Structure of active β-arrestin-1 bound to a G-protein-coupled receptor phosphopeptide. Nature *497*, 137–141. 10.1038/nature12120.
61. Nguyen, A.H., Thomsen, A.R.B., Cahill 3rd, T.J., Huang, R., Huang, L.Y., Marcink, T., Clarke, O.B., Heissel, S., Masoudi, A., Ben-Hail, D., et al. (2019). Structure of an endosomal signaling GPCR-G protein-beta-arrestin megacomplex. Nat Struct Mol Biol *26*, 1123–1131. 10.1038/s41594-019-0330-y.
62. Aydin, Y., Böttke, T., Lam, J.H., Ernicke, S., Fortmann, A., Tretbar, M., Zarzycka, B., Gurevich, V. V., Katritch, V., and Coin, I. (2023). Structural details of a Class B GPCR-arrestin complex revealed by genetically encoded crosslinkers in living cells. Nat Commun *14*. 10.1038/s41467-023-36797-2.
63. He, Q.-T., Xiao, P., Huang, S.-M., Jia, Y.-L., Zhu, Z.-L., Lin, J.-Y., Yang, F., Tao, X.-N., Zhao, R.-J., Gao, F.-Y., et al. (2021). Structural studies of phosphorylation-dependent interactions between the V2R receptor and arrestin-2. Nat Commun *12*, 2396. 10.1038/s41467-021-22731-x.
64. Van Roey, K., Gibson, T.J., and Davey, N.E. (2012). Motif switches: decision-making in cell regulation. Curr Opin Struct Biol *22*, 378–385. 10.1016/j.sbi.2012.03.004.
65. Lee, C.W., Ferreon, J.C., Ferreon, A.C.M., Arai, M., and Wright, P.E. (2010). Graded enhancement of p53 binding to CREB-binding protein (CBP) by multisite phosphorylation. Proc Natl Acad Sci U S A *107*, 19290–19295. 10.1073/pnas.1013078107.
66. Zosel, F., Holla, A., and Schuler, B. (2022). Labeling of Proteins for Single-Molecule Fluorescence Spectroscopy. In Protein Folding: Methods and Protocols, V. Muñoz, ed. (Springer US), pp. 207–233. 10.1007/978-1-0716-1716-8_12.
67. Chemes, L.B., Alonso, L.G., Noval, M.G., and de Prat-Gay, G. (2012). Circular Dichroism Techniques for the Analysis of Intrinsically Disordered Proteins and Domains. In Intrinsically Disordered Protein Analysis: Volume 1, Methods and Experimental Tools Methods in Molecular Biology., V. N. Uversky and A. K. Dunker, eds. (Humana Press), pp. 387–404.
68. Thureau, A., Roblin, P., and Pérez, J. (2021). BioSAXS on the SWING beamline at Synchrotron SOLEIL. J Appl Crystallogr *54*, 1698–1710. 10.1107/s1600576721008736.
69. Blanchet, C.E., and Svergun, D.I. (2013). Small-angle X-ray scattering on biological macromolecules and nanocomposites in solution. Annu Rev Phys Chem *64*, 37–54. 10.1146/annurev-physchem-040412-110132.
70. Panjkovich, A., and Svergun, D.I. (2018). CHROMIXS : automatic and interactive analysis of chromatography-coupled small-angle X-ray scattering data. Structural bioinformatics *34*, 1944–1946. 10.1093/bioinformatics/btx846.
71. Wishart, D.S., and Sykes, B.D. (1994). Chemical shifts as a tool for structure determination. Methods Enzymol *239*, 363–392. 10.1016/S0076-6879(94)39014-2.

72. Lee, W., Tonelli, M., and Markley, J.L. (2015). NMRFAM-SPARKY: enhanced software for biomolecular NMR spectroscopy. Bioinformatics *31*, 1325–1327. 10.1093/bioinformatics/btu830.

73. Vuister, G.W., and Bax, A. (1993). Quantitative J correlation: a new approach for measuring homonuclear three-bond J(HNH.alpha.) coupling constants in 15N-enriched proteins. J Am Chem Soc *115*, 7772–7777. 10.1021/ja00070a024.

74. Ottiger, M., Delaglio, F., and Bax, A. (1998). Measurement ofJand Dipolar Couplings from Simplified Two-Dimensional NMR Spectra. Journal of Magnetic Resonance *131*, 373–378. https://doi.org/10.1006/jmre.1998.1361.

75. Rückert, M., and Otting, G. (2000). Alignment of Biological Macromolecules in Novel Nonionic Liquid Crystalline Media for NMR Experiments. J Am Chem Soc *122*, 7793–7797. 10.1021/ja001068h.

76. Hansen, M.R., Mueller, L., and Pardi, a (1998). Tunable alignment of macromolecules by filamentous phage yields dipolar coupling interactions. Nat Struct Biol *5*, 1065–1074. 10.1038/4176.

77. Teilum, K., Kragelund, B.B., and Poulsen, F.M. (2002). Transient Structure Formation in Unfolded Acyl-coenzyme A-binding Protein Observed by Site-directed Spin Labelling. J Mol Biol *324*, 349–357. 10.1016/S0022-2836(02)01039-2.

78. Grzesiek, S., Bax, A., Clore, G.M., Gronenborn, A.M., Hu, J.-S., Kaufman, J., Palmer, I., Stahl, S.J., and Wingfield, P.T. (1996). The solution structure of HIV-1 Nef reveals an unexpected fold and permits delineation of the binding surface for the SH3 domain of Hck tyrosine protein kinase. Nat Struct Mol Biol *3*, 340–345. 10.1038/nsb0496-340.

79. Ozenne, V., Bauer, F., Salmon, L., Huang, J. -r., Jensen, M.R., Segard, S., Bernado, P., Charavay, C., and Blackledge, M. (2012). Flexible-meccano: a tool for the generation of explicit ensemble descriptions of intrinsically disordered proteins and their associated experimental observables. Bioinformatics *28*, 1463–1470. 10.1093/bioinformatics/bts172.

80. Granier, S., Kim, S., Shafer, A.M., Ratnala, V.R.P., Fung, J.J., Zare, R.N., and Kobilka, B. (2007). Structure and conformational changes in the C-terminal domain of the beta2-adrenoceptor: insights from fluorescence resonance energy transfer studies. J Biol Chem *282*, 13895–13905. 10.1074/jbc.M611904200.

81. Bernado, P., Mylonas, E., Petoukhov, M. V, Blackledge, M., and Svergun, D.I. (2007). Structural characterization of flexible proteins using small-angle X-ray scattering. J Am Chem Soc *129*, 5656–5664. 10.1021/ja069124n.

82. Tria, G., Mertens, H.D.T., Kachala, M., and Svergun, D.I. (2015). Advanced ensemble modelling of flexible macromolecules using X-ray solution scattering. IUCrJ *2*, 207–217. 10.1107/S205225251500202X.

83. Hess, B., Bekker, H., Berendsen, H.J.C., and Fraaije, J.G.E.M. (1997). LINCS: A Linear Constraint Solver for molecular simulations. J Comput Chem *18*, 1463–1472. 10.1002/(SICI)1096-987X(199709)18:12<1463::AID-JCC4>3.0.CO;2-H.

84. Darden, T., York, D., and Pedersen, L. (1993). Particle mesh Ewald: An N·log(N) method for Ewald sums in large systems. J Chem Phys *98*, 10089–10092. 10.1063/1.464397.
85. Nosé, S. (1984). A unified formulation of the constant temperature molecular dynamics methods. J Chem Phys *81*, 511–519. 10.1063/1.447334.
86. Parrinello, M., and Rahman, A. (1981). Polymorphic transitions in single crystals: A new molecular dynamics method. J Appl Phys *52*, 7182–7190. 10.1063/1.328693.

SUPPLEMENTAL INFORMATION

Phosphorylation motif dictates GPCR C-terminal domain conformation and arrestin interaction

Myriam Guillien,[1,†] Assia Mouhand,[1,†] Amin Sagar,[1] Aurélie Fournet,[1] Frédéric Allemand,[1] Glaécia A. N. Pereira,[2] Aurélien Thureau,[3] Pau Bernadó,[1] Jean-Louis Banères,[2] Nathalie Sibille,[1,4,*]

[1]Centre de Biologie Structurale (CBS), CNRS, Univ. Montpellier, Inserm, Montpellier, France
[2]Institut des Biomolécules Max Mousseron (IBMM), UMR-5247, Univ. Montpellier, CNRS, ENSCM, Montpellier, France
[3]HélioBio Section, Synchrotron SOLEIL, L'Orme des Merisiers, Saint-Aubin BP 48, 91190 Gif-sur-Yvette, France

[4]Lead contact
† These authors contributed equally to this work

*Correspondence: nathalie.sibille@cbs.cnrs.fr

Protein	3D	$^{3}J_{HNHA}$	Relaxation	RDC alcohol	RDC Pf1	PRE
pm-V2R	50	93	93	93	138	NT
pm-GHSR	377	263	263	263	250	NT
pm-β2AR	206	476	476	476	212	100

Table S1. Concentration used for the NMR characterization of phosphomimetic GPCR C-termini of V2R-Cter (blue), GHSR-Cter (green) and β2AR-Cter (pink), Related to Figure 2
Concentration used in each experiment is indicated in μM. The letters NT mean that these experiments have not been carried out.

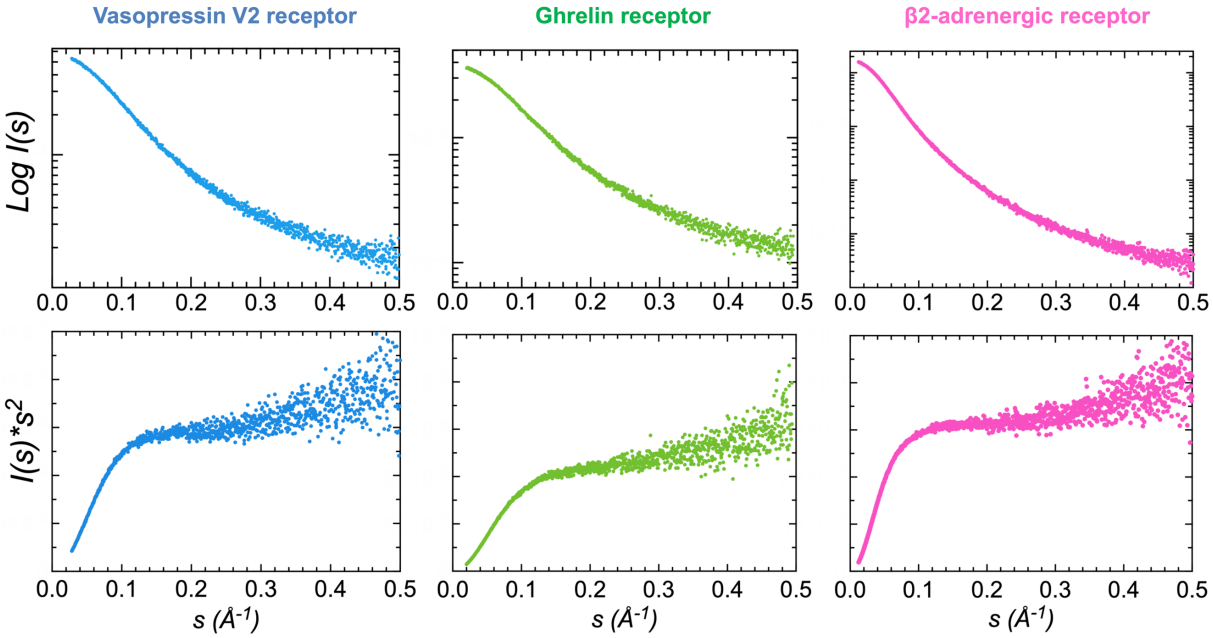

Figure S1. SAXS data of phosphomimetic variants of V2R-Cter (blue, left), GHSR-Cter (green, middle) and β2AR-Cter (pink, right), Related to Figure 1

Semi-logarithmic representation of the experimental SAXS curves versus scattering angle (upper panel) and Kratky plots (lower panel). The Kratky plot of variants display a typical profile of IDP with no clear maximum and a monotone increase along the momentum transfer range[1–3].

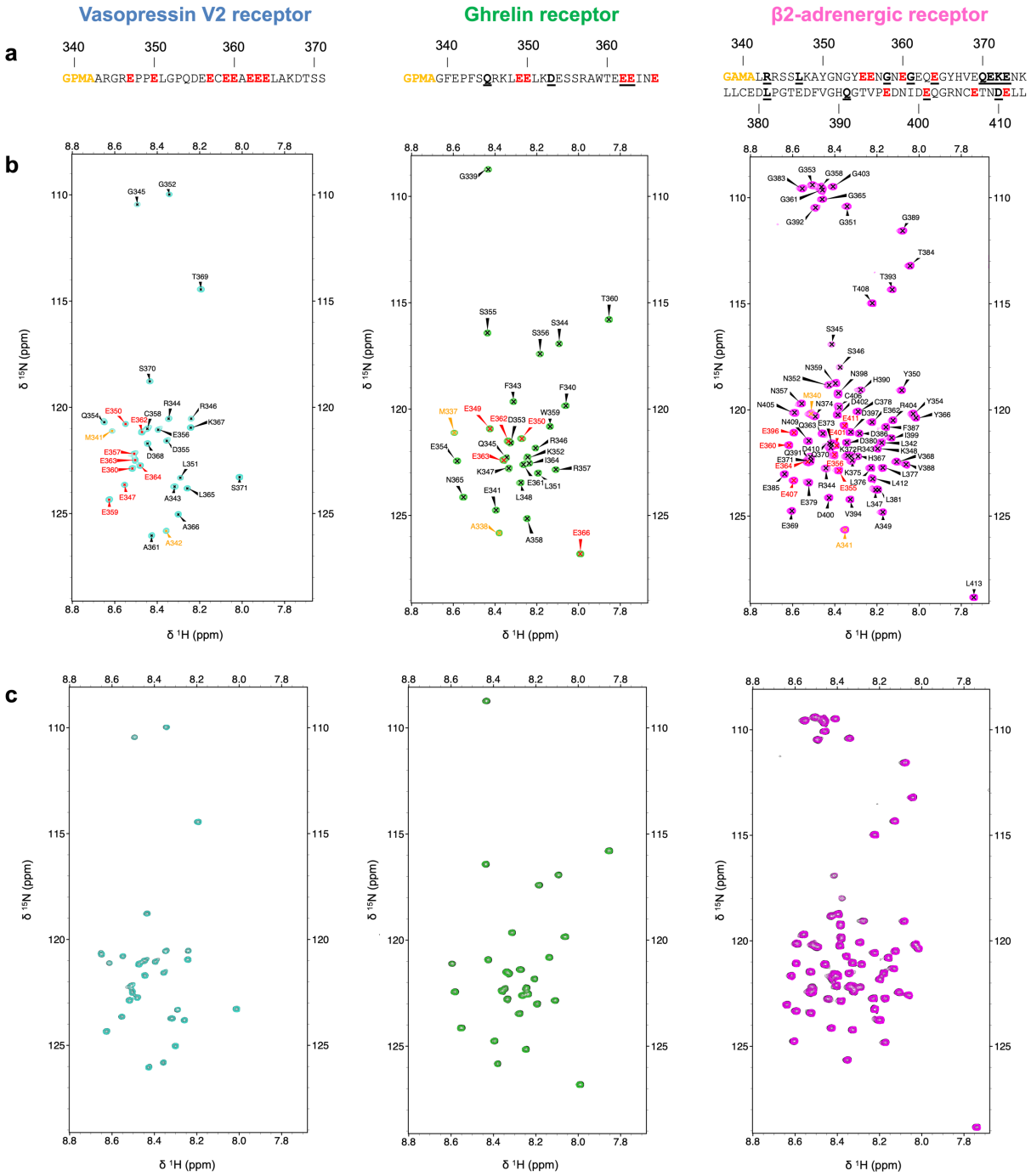

Figure S2. Assignments of phosphomimetic variants of V2R-Cter (blue, left), GHSR-Cter (green, middle) and β2AR-Cter (pink, right), Related to Fig. 2b

a Sequence of the phosphomimetic C-terminal domains with known phosphorylation sites mutated by glutamic acid (E) indicated in red. Amino acids coming from the protease cleavage site are shown in orange and overlapping residues are underlined in black.

b ^{15}N-HSQC of the C-terminal domains were recorded on 300 µM samples at 700 MHz, 20 °C, in 50 mM Bis-Tris pH 6.7, 150 mM NaCl buffer. Residue-specific assignments are shown on spectra and are colored according to **a**.

c Overlay of ^{15}N-HSQCs recorded on samples at 300 µM (black) or 100 µM (colored) at 700 MHz, 20 °C, 50 mM Bis-Tris pH 6.7, 150 mM NaCl of V2R-Cter (blue, left), GHSR-Cter (green, middle) and β2AR-Cter (pink, right). No chemical shift changes were observed in NMR spectra at different concentrations. Thus, the spectrum at 300 µM (black) is hidden by the spectrum at 100 µM (colored). The concentration of pm-GPCR-Cters doesn't affect their conformations.

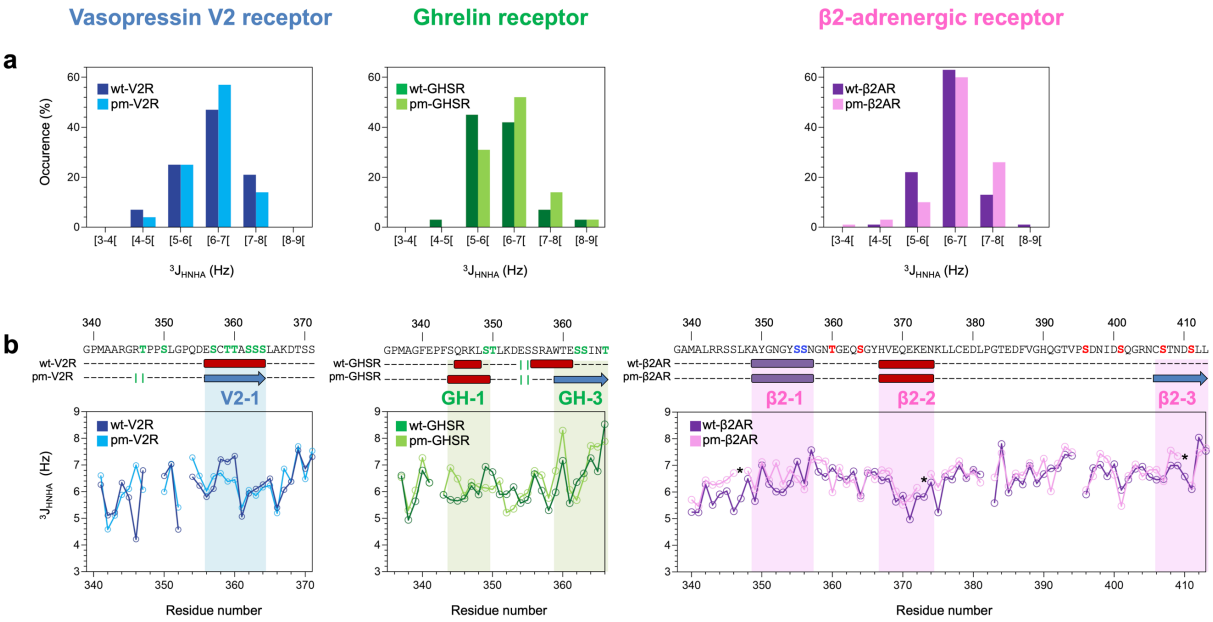

Figure S3. Overlay of 3JHNHA scalar coupling of wild type (dark color, data previously shown [4]) and phosphomimetic variant (light color) form of V2R-Cter (blue, left); GHSR-Cter (green, middle) and β2AR-Cter (purple, right), Related to Figure 2

a Histogram of the 3JHNHA in Hz. The couplings seem to shift to higher values in the variant suggesting a lower content of helical conformation (values below 6 Hz) and a higher content of extended conformation (values above 8 Hz).

b On top, sequence and NMR secondary structure consensus of GPCR C-termini are shown according to figure 2. Below, the coupling values along the sequence are represented. For β2AR variant, outlier values for overlapping residues in HSQCs were removed (dark stars). They were recorded at 700 MHz, 20 °C, 50 mM Bis-Tris pH 6.7, 150 mM NaCl.

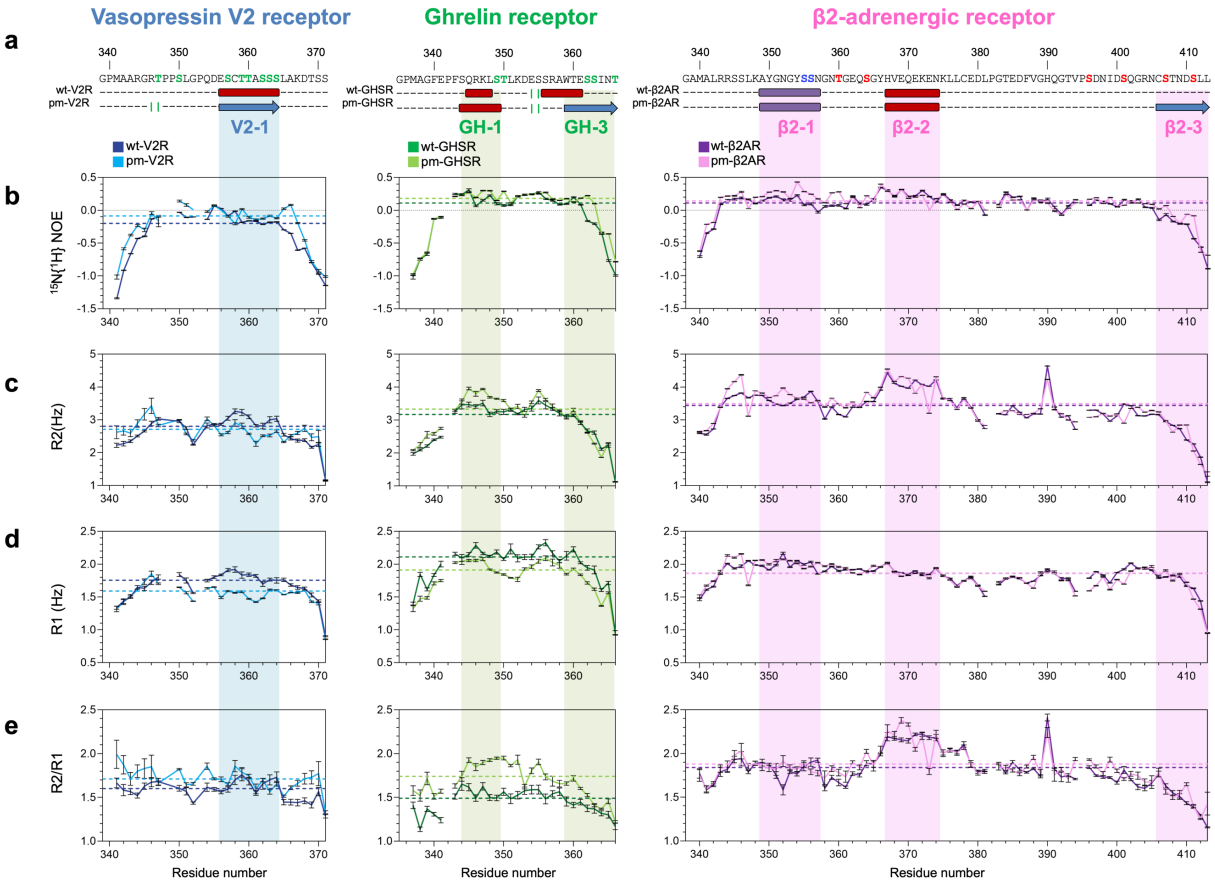

Figure S4. Overlay of relaxation data of wild type (dark color, data previously shown [4]) and variant (light color) forms of V2R-Cter (blue, left); GHSR-Cter (green, middle) and β2AR-Cter (purple/pink, right), Related to Figure 2c

a Sequence and NMR secondary structure consensus of GPCR C-termini are shown according to Fig. 2.

b $^{15}N\{^{1}H\}$ heteronuclear NOE.

c Transversal relaxation rates R2.

d Longitudinal relaxation rates R1; and **e** R2/R1 ratio are shown in colored line. Average values are indicted by dashed colored line. Relaxation data were recorded at 700 MHz, 20 °C, in 50 mM Bis-Tris pH 6.7, 150 mM NaCl buffer.

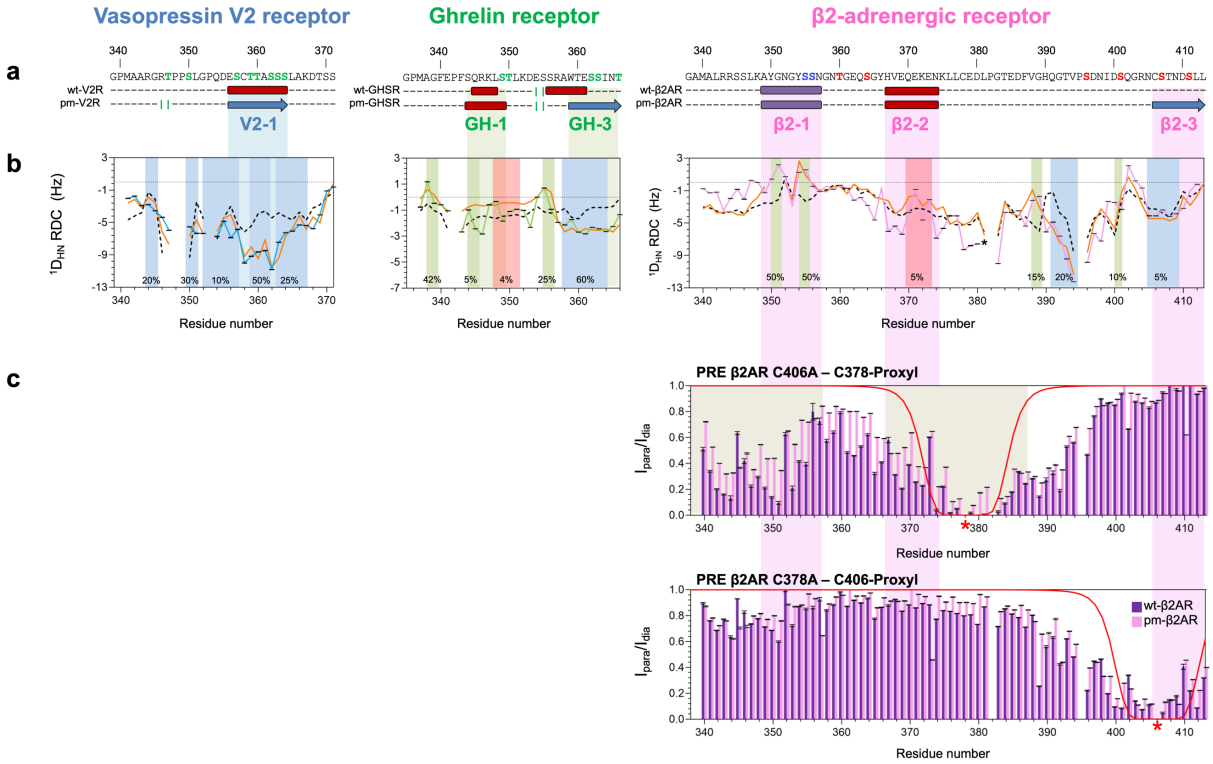

Figure S5. $^1D_{NH}$ RDCs values and PRE data used in the ensemble description [5] of wild type (dark color, data previously shown [4]) and phosphomimetic variant (light color) forms for V2R-Cter (blue, left); GHSR-Cter (green, middle) and β2AR-Cter (purple/pink, right), Related to Figure 2d

a Sequence and NMR secondary structure consensus of GPCR-Cters are shown according to Figure 2.

b Comparison of experimental RDCs values (full line) measured in bacteriophage Pf1 for pm-GHSR-Cter, and alcohol mixture for pm-V2R-Cter and pm-β2AR-Cter with back-calculated RDC computed by FM on random-coil (black dash line), or on biased ensemble (orange line) populated as indicated in the figure (regions colored in red (helical structure), blue (extended structure) or green (turn). Outliers due to overlapping residues were removed (dark star). Data are represented as mean ± SD.

c PRE data of C406A variant labeled on C378 (red star). Reduction of the intensity ratio suggests long-range interaction in regions highlighted in grey, which has been used for FM building of pm-β2AR-Cter and wt-β2AR-Cter [4] ensembles. PRE data of C378E variant labeled on C406 (red star). PREs were calculated from the ratio of intensity (I_{para}/I_{dia}) of ^{15}N-HSQC spectra measured for the paramagnetic (I_{para}) sample (position of PROXYL probe is indicated with a red star), and for the diamagnetic sample (I_{dia}). They were recorded at 700 MHz, 20 °C, in 50 mM Bis-Tris pH 6.7, 150 mM NaCl buffer, on sample at 50 µM for wt-β2AR-Cter and 100 µM for pm-β2AR-Cter. Theoretical PRE curves for a completely disordered protein are shown in red. Data are represented as mean ± SD.

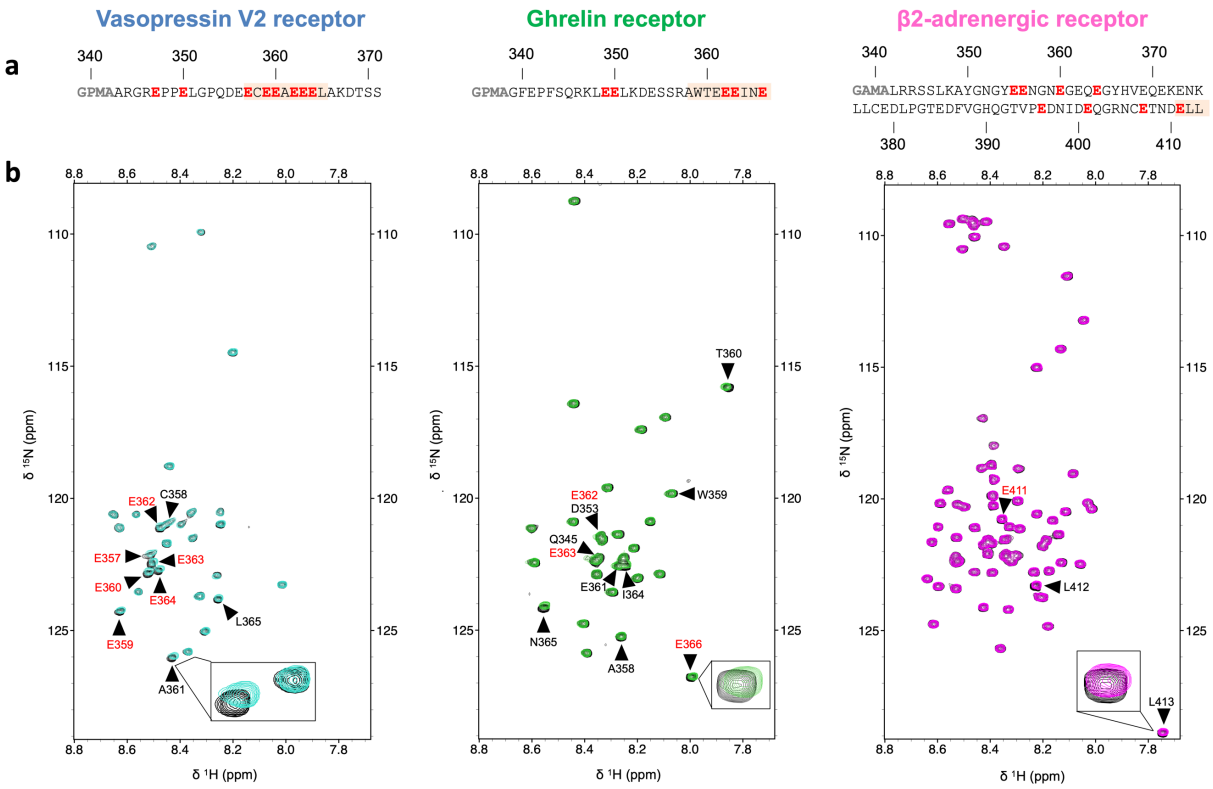

Figure S6. Visualization of pm-GPCR-C-ter:arrestin interaction by NMR of V2R-Cter (blue, left), GHSR-Cter (green, middle) and β2AR-Cter (pink, right), Related to Figure 3

a Sequence of the GPCR C-termini. Glutamic acid residues that mimic GRK phosphorylation sites are indicated in red. Binding regions are highlighted in orange.

b Overlay of ^{15}N-HSQC spectra without arrestin (in black) and with arrestin at ratio 1:10 (in color). Residues involved in the interaction are noted in black or red according to **a**. Spectra were recorded on ^{15}N labeled Cter samples at 10 µM with 0 or 100 µM of unlabeled arrestin at 800 MHz, 20 °C, 50 mM Bis-Tris pH 6.7, 50 mM NaCl.

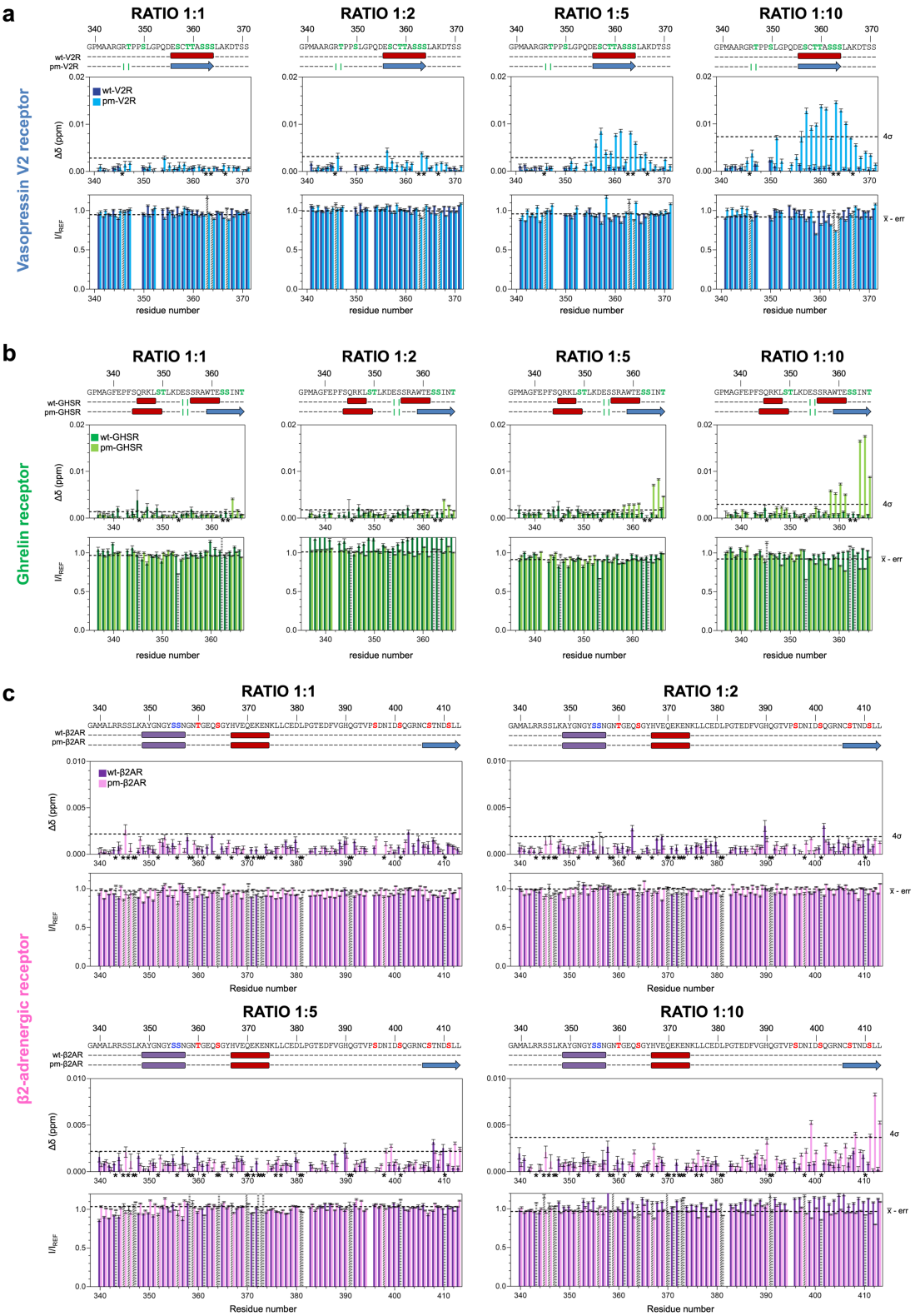

Figure S7. Interaction by NMR between arrestin-2 and (a) wt-V2R-Cter (dark blue) or pm-V2R-Cter (light blue), (b) wt-GHSR-Cter (dark green) or pm-GHSR-Cter (light green) and (c) wt-β2AR-Cter (purple) or pm-β2AR-Cter (pink) at different ratios, Related to Figure 3

For each C-terminus, the sequence and NMR secondary structure consensus are indicated according to Fig. 2. Below, histogram of $^{1}H/^{15}N$ chemical shift changes and intensity ratios (I/I_{REF}) are shown. Cut-off are indicated in black, dashed line and on the right. In the histogram of chemical shit changes, overlapping residues in HSQCs were removed and are shown in black stars near residues numbers. In the histogram of intensity ratio, they are represented in dashed bars. Spectra were recorded at 800 MHz, 20 °C, 50 mM Bis-Tris pH 6.7, 50 mM NaCl, on ^{15}N Cter samples at 10 µM C-termini with 0, 10, 20, 50 or 100 µM of unlabeled arrestin. Data are represented as mean ± SD.

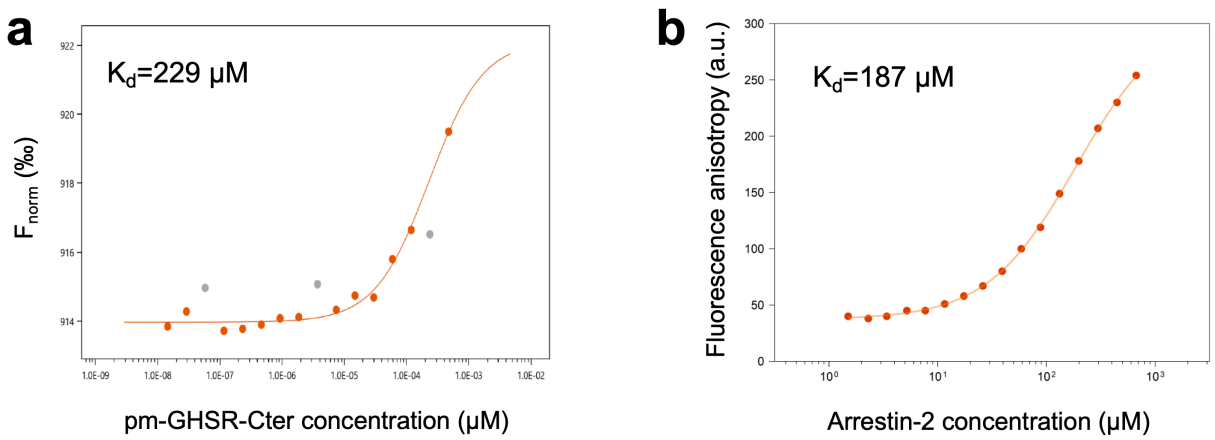

Figure S8. Low affinity interaction between arrestin-2 and the C-terminus of GHSR phosphomimetic, Related to Figure 5

a Dose-response curve of the Micro-Scale Thermophoresis (MST) titration. Labeled arrestin-2 at 5 nM was incubated with GHSR peptide (from 0.01 to 450 µM), at pH 6.7, 20 °C, 50 mM NaCl. An MST on-time of 5 sec was used for analysis and a dissociation constant (K_D) of 229 µM was obtained. Three data points were removed from the calculation (grey dots).

b Fluorescence anisotropy curve. Labeled GHSR was incubated with varying amounts of arrestin-2: from 0 to 670 µM, at pH 6.7, 20 °C, 50 mM NaCl. A 187 µM dissociation constant (K_D) was determined. We could not measure KDs of arrestin2 with (i) V2R-Cter due to unspecific capillary interaction, and (ii) B2AR-Cter due to its extremely weak affinity.

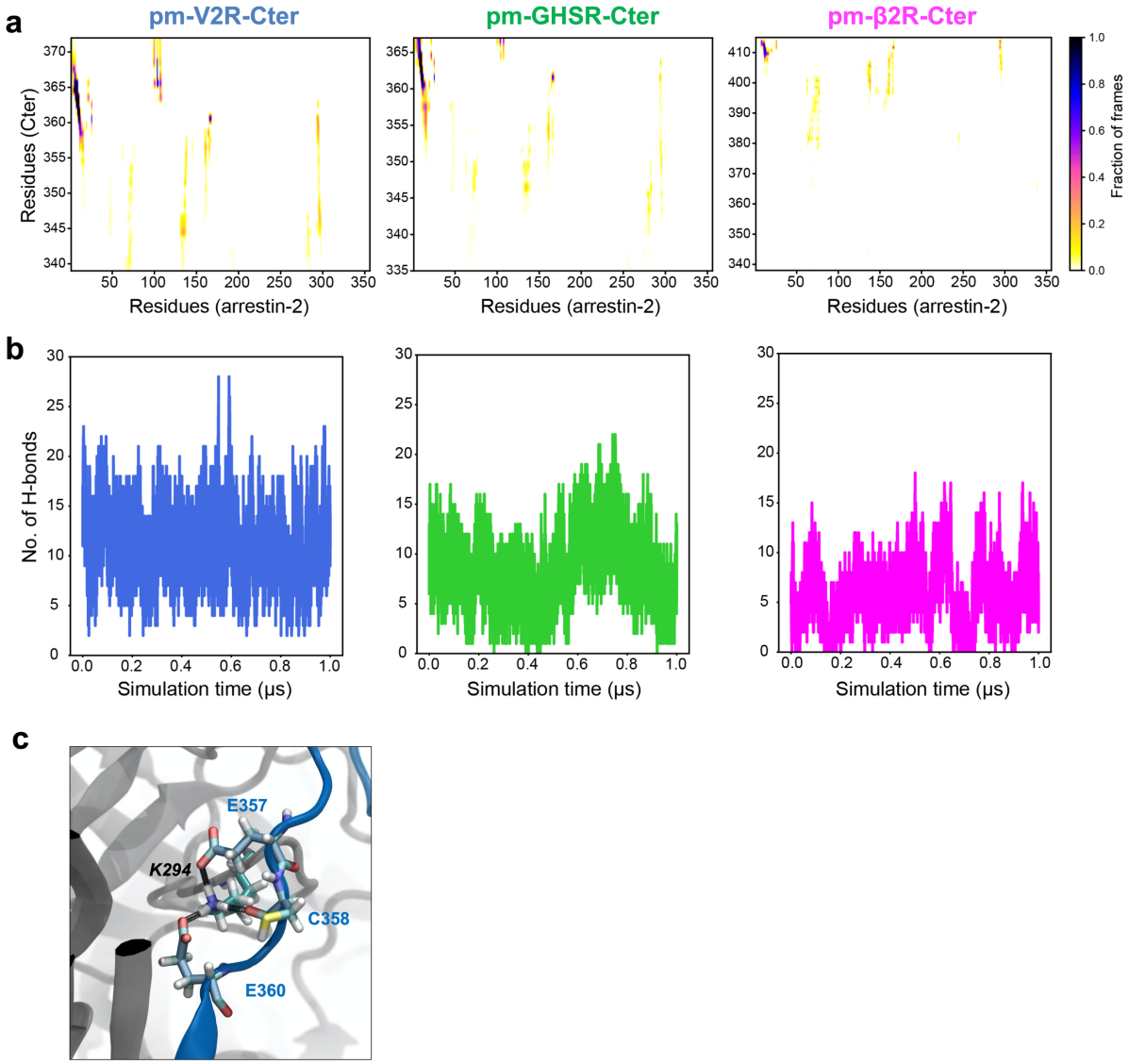

Figure S9. Interaction analysis of pm-V2R-Cter (blue), pm-GHSR-Cter (green) and pm-β2AR-Cters (pink): arrestin (grey) modeling complexes, Related to Figure 6
a The lifetime of contacts between residues of arrestin-2 (X-axis) and C-ters (Y-axis).
b The number of hydrogen bonds between the Cters and arrestin through the concatenated simulations trajectories.
c The bifurcated salt-bridge formed by E357 and E360 of pm-V2R-Cter with K294 of arrestin-2 along with an additional H-bond with C358 (pm-V2R-Cter)

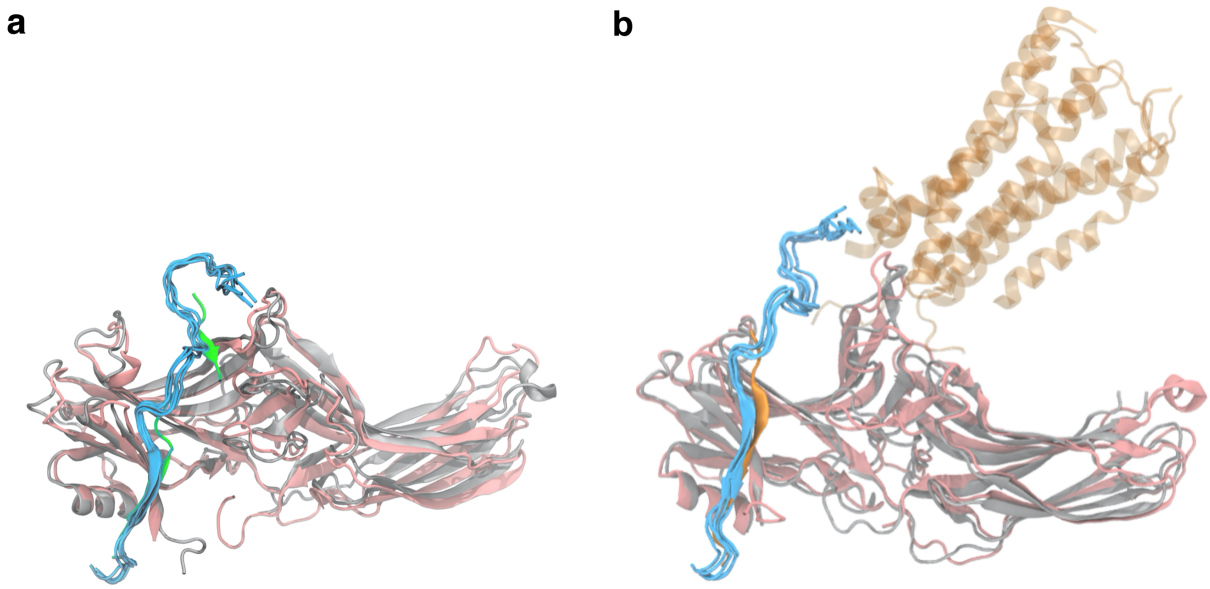

Figure S10. Atomic structures of pm-V2R-Cter and entire V2 receptor complexed with arrestin, Related to Figure 4

Four selected peptide conformation from an ensemble obtained from MD simulations of pm-V2R-Cter (light blue) complexed to arrestin (pink) superimposed to

a the X-ray structure of the V2Rpp (green, PDB code 4JQI)

b the cryo-EM structure of the entire V2 receptor (orange, PDB code 7R0J), complexed to arrestin (grey).

REFERENCES

1. Sibille, N., and Bernadó, P. (2012). Structural characterization of intrinsically disordered proteins by the combined use of NMR and SAXS. Biochem Soc Trans *40*, 956–962. 10.1042/BST20120149.
2. Cordeiro, T.N., Herranz-Trillo, F., Urbanek, A., Estaña, A., Cortés, J., Sibille, N., and Bernadó, P. (2017). Structural characterization of highly flexible proteins by small-angle scattering. In Advances in Experimental Medicine and Biology (Springer New York LLC), pp. 107–129. 10.1007/978-981-10-6038-0_7.
3. Cordeiro, T.N., Herranz-Trillo, F., Urbanek, A., Estaña, A., Cortés, J., Sibille, N., and Bernadó, P. (2017). Small-angle scattering studies of intrinsically disordered proteins and their complexes. Curr Opin Struct Biol *42*, 15–23. 10.1016/j.sbi.2016.10.011.
4. Guillien, M., Mouhand, A., Fournet, A., Gontier, A., Thureau, A., Allemand, F., Banères, J.-L., Bernadó, P., and Sibille, N. (2022). Structural insights into the intrinsically disordered GPCR C-terminal region, major actor in arrestin-GPCR interaction. Biomolecules *12*, 617. 10.3390/biom12050617.
5. Delaforge, E., Cordeiro, T.N., Bernadó, P., and Sibille, N. (2018). Conformational characterization of intrinsically disordered proteins and its biological significance. In Modern Magnetic Resonance (Springer International Publishing), pp. 381–399. 10.1007/978-3-319-28388-3_52.